Author Manuscript

Author Manuscript

Author Manuscript

Author Manuscript

HHS Public Access

Author manuscript

Cell Rep. Author manuscript; available in PMC 2022 February 14.

Published in final edited form as:

Cell Rep. 2021 March 23; 34(12): 108896. doi:10.1016/j.celrep.2021.108896.

EGF-mediated suppression of cell extrusion during mucosal damage attenuates opportunistic fungal invasion

Sebastian Wurster[1,7], **Oscar E. Ruiz**[2,7], **Krystin M. Samms**[2], **Alexander M. Tatara**[3], **Nathaniel D. Albert**[1], **Philip H. Kahan**[2], **Anh Trinh Nguyen**[4,5], **Antonios G. Mikos**[6], **Dimitrios P. Kontoyiannis**[1,7,*], **George T. Eisenhoffer**[2,5,7,8,*]

[1]Department of Infectious Diseases, Infection Control and Employee Health, The University of Texas MD Anderson Cancer Center, Houston, TX, USA

[2]Department of Genetics, The University of Texas MD Anderson Cancer Center, Houston, TX, USA

[3]Medical Scientist Training Program, Baylor College of Medicine, Houston, TX, USA

[4]Department of Microbiology and Molecular Genetics, McGovern Medical School, University of Texas Health Science Center, Houston, TX, USA

[5]MD Anderson Cancer Center UTHealth Graduate School of Biomedical Sciences, Houston, TX, USA

[6]Department of Bioengineering, Rice University, Houston, TX, USA

[7]These authors contributed equally

[8]Lead contact

SUMMARY

Severe and often fatal opportunistic fungal infections arise frequently following mucosal damage caused by trauma or cytotoxic chemotherapy. Interaction of fungal pathogens with epithelial cells that comprise mucosae is a key early event associated with invasion, and, therefore, enhancing epithelial defense mechanisms may mitigate infection. Here, we establish a model of mold and yeast infection mediated by inducible epithelial cell loss in larval zebrafish. Epithelial cell loss by extrusion promotes exposure of laminin associated with increased fungal attachment, invasion, and larval lethality, whereas fungi defective in adherence or filamentation have reduced virulence. Transcriptional profiling identifies significant upregulation of the epidermal growth

This is an open access article under the CC BY-NC-ND license (http://creativecommons.org/licenses/by-nc-nd/4.0/).

*Correspondence: dkontoyi@mdanderson.org (D.P.K.), gteisenhoffer@mdanderson.org (G.T.E.).

AUTHOR CONTRIBUTIONS

D.P.K. and G.T.E. conceived of the study. S.W. and O.E.R. performed all experiments and subsequent analyses. A.M.T. optimized the fungal infection assay. K.M.S. performed imaging and cell tracking analyses. A.T.N. assisted with live imaging of the fungal/neutrophil interface. P.H.K. and N.D.A. provided key technical support. A.G.M. helped to develop the initial fungal infection plat form. S.W., O.E.R., D.P.K., and G.T.E. wrote the manuscript.

DECLARATION OF INTERESTS

D.P.K. reports research support from Astellas Pharma and honoraria for lectures or consultantships from Merck & Co., Astellas Pharma, Gilead Sciences, Mayne Pharmaceuticals, Amplyx Pharmaceuticals, and Pulmocide, Inc.

SUPPLEMENTAL INFORMATION

Supplemental information can be found online at https://doi.org/10.1016/j.celrep.2021.108896.

Author Manuscript Author Manuscript Author Manuscript Author Manuscript

factor receptor ligand *epigen* (EPGN) upon mucosal damage. Treatment with recombinant human EPGN suppresses epithelial cell extrusion, leading to reduced fungal invasion and significantly enhanced survival. These data support the concept of augmenting epithelial restorative capacity to attenuate pathogenic invasion of fungi associated with human disease.

In brief

Wurster et al. show that extrusion of numerous epithelial cells from tissue can expose underlying extracellular matrix components to promote increased attachment and invasion of fungi associated with human disease. Treatment with recombinant human EPGN suppressed epithelial cell extrusion, leading to significantly reduced opportunistic fungal invasion.

Graphical abstract

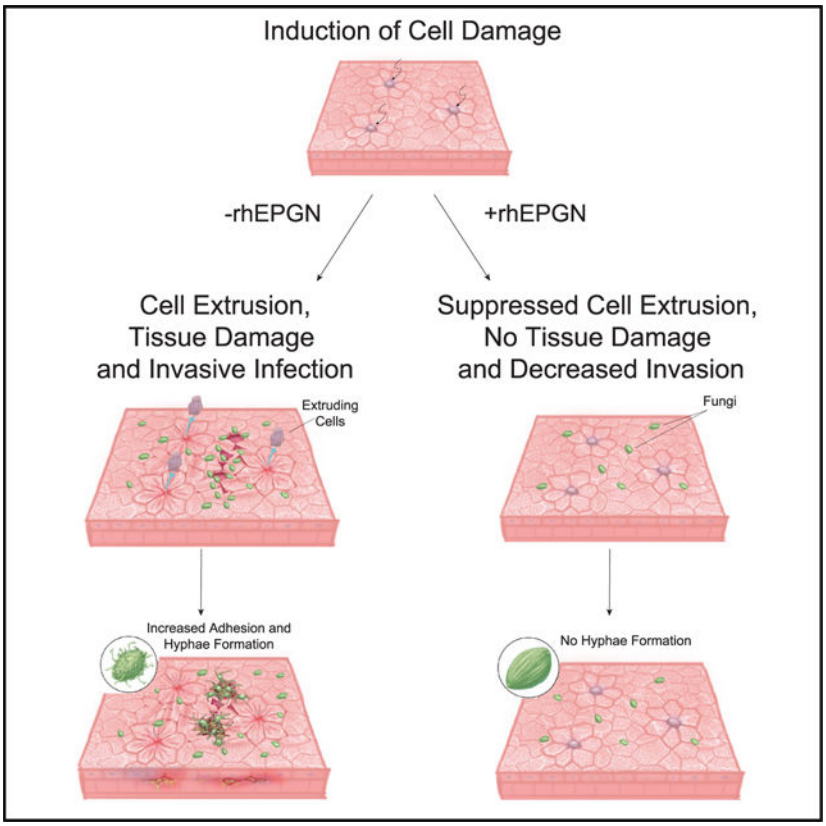

INTRODUCTION

Formation and maintenance of an epithelial barrier is essential for defense against pathogens and other noxious stimuli and is fundamental for the survival of all animals (Hooper, 1956; Pellettieri and Sánchez Alvarado, 2007). Compromised epithelial integrity following trauma is a common mode of infection by opportunistic molds, such as Mucorales (Ibrahim et al., 2012; Ibrahim and Voelz, 2017). Damage to mucosal epithelia following cytotoxic chemotherapy, a condition referred to as mucositis (Naidu et al., 2004), is considered the most common portal of entry of *Candida* species, resulting in invasive candidiasis

Author Manuscript Author Manuscript Author Manuscript Author Manuscript

(Pfaller and Diekema, 2007; Rodrigues et al., 2019; Sipsas and Kontoyiannis, 2012). Despite interaction of fungal pathogens with epithelial cells being a key early event associated with invasion (Ibrahim and Voelz, 2017; Koh et al., 2008), little is known about how disruption of homeostatic mechanisms in living mucosa may facilitate fungal pathogenesis.

The technical challenge of perturbing living epithelia in the presence of fungi and imaging subsequent changes *in vivo* and in real time has so far prevented detailed characterization of how tissue damage can contribute to invasive fungal disease. To overcome these limitations, here we expose zebrafish larvae to different opportunistic fungal pathogens after inducing epithelial cell loss and define fungal interactions with damaged mucosae during invasion. The larval zebrafish epidermis is a bilayer positioned on top of a basement membrane (Dane and Tucker, 1985; Eisenhoffer et al., 2017; Le Guellec et al., 2004; Webb and Kimelman, 2005) and consists of cells that express markers similar to epithelia of the oral cavity, airway, and urogenital track in mammals (Chen et al., 2005; Claudinot et al., 2020; Pignon et al., 2013; Rock et al., 2010). Utilizing a combinatorial approach with *in vivo* time-lapse imaging and assessment of adhesion- and filamentation-defective fungal mutants, we demostrate that loss of many epithelial cells by extrusion can expose underlying extracellular matrix components that facilitate adhesion and invasion of molds (e.g., *Rhizopus arrhizus)* and yeast (e.g., *Candida albicans*) associated with human disease. We show that suppressing cell extrusion by treatment with the human recombinant epidermal growth factor ligand epigen (EPGN) preserves tissue integrity in the face of damage and is able to reduce fungal invasion and significantly improve larval survival. This study provides key insights into the mechanisms by which epithelial cell loss and mucosal injury drive opportunistic fungal infections.

RESULTS

A model of invasive fungal infection mediated by inducible epithelial cell loss

To examine fungal interactions with intact and damaged living mucosal tissues, we induced damage in a subset of surface epithelial cells in the zebrafish epidermis (Brock et al., 2019; Eisenhoffer et al., 2017) to promote mucosal breach and then immersed the larvae in media containing fungi associated with human disease (Figure 1A). We first generated an inducible model of mucosal epithelial tissue damage by expressing the bacterial enzyme nitroreductase (*nfsB*; referred to as NTR) tagged with mCherry fluorescent protein (Curado et al., 2008; Davison et al., 2007) in the surface epithelial cells of zebrafish using the *zc1044a* GAL4 enhancer trap line. Addition of metronidazole (MTZ) to 4 days post fertilization (4 dpf) larvae caused a NTR-dependent conversion of MTZ to a cytotoxic agent and induced rapid elimination of apoptotic surface epithelial cells by extrusion, a homeostatic mechanism used to remove unfit or aberrant cells (Atieh et al., 2020; Eisenhoffer et al., 2012; Rosenblatt et al., 2001; Figures 1B–1E; Figures S1A–S1H). Notably, this treatment caused significant morphological changes to the tail fin epithelium and oral mucosa, mimicking chemotherapy-associated mucosal tissue damage.

We next observed the interaction of the most common pathogenic Mucorales species, *Rhizopus arrhizus* (FTR1-GFP-*R. arrhizus*), with the larval epidermis (mCherry-nfsB) under homeostatic conditions and after induction of mucosal damage (Figures 1F–1I). After

Author Manuscript Author Manuscript Author Manuscript Author Manuscript

5-h MTZ treatment and overnight exposure to the fungus (16–18 h post infection [hpi]), hyphae were present on the tail fin epithelium and oral mucosa, areas where cell loss was observed (Figures 1H and 1I). In contrast, minimal *Rhizopus* spore attachment was found when epithelial integrity was intact (homeostatic conditions), and no invasive hyphae were detected (Figures 1F and 1G). The morphological changes to the mouth and tail fin after mucosal damage correlated with a time-dependent decline in survival rates of *R. arrhizus*-infected larvae ($p < 0.001$, Mantel-Cox log-rank test from 3 independent experiments with a total of 25–28 larvae per condition; Figure 1J). In line with these results, exposure to different MTZ concentrations promoted a concentration-dependent increase in the number of extruding apoptotic surface cells (Figures S1F–S1H) that also correlated with larval mortality upon *R. arrhizus* infection (Figure 1K). In contrast, increasing mucosal damage did not result in increased mortality in the absence of infection (Figure S1E). Similarly, exposure of larvae with epithelial cell loss to differential amounts of *R. arrhizus* spores revealed significant inoculum dependency of survival rates (Figure 1L) and fungal tissue burden, as determined by detection of *R. arrhizus* gene copies from infected larvae (Figure S2A).

To rule out that increased mortality after infection and tissue damage was caused by an inflammatory response because of adherence and exposure to fungi, we performed mock infection using heat-killed *R. arrhizus*. Even at a concentration of 5×10^7 inactivated spores/mL, 95% survival was observed 72 h after exposure of larvae with mucosal damage (Figure 1M). Moreover, addition of heat-killed spores to a sub-lethal inoculum of vital spores did not increase mortality of larvae with mucosal damage (Figures S2B and S2C). To demonstrate the generalizability of our findings, we also confirmed inoculum-dependent mortality for *Mucor circinelloides*, the second most common cause of mucormycosis (Farmakiotis and Kontoyiannis, 2016), as well *Candida albicans*, the most common human fungal pathogen (Figures S2D and S2E). We conclude, from these results, establishment of an immersion-based vertebrate infection model that is mediated by epithelial cell loss and mucosal damage and is applicable to different classes of opportunistic fungal pathogens.

Spatial and temporal events driving invasive fungal infection after epithelial cell extrusion

To define the spatial and temporal events that occur in *R. arrhizus*-infected larvae upon epithelial damage, we performed fixed tissue analysis and time-lapse imaging and found that spore attachment to the larval epidermis occurred after 2–6 hpi primarily at sites with increased epithelial cell loss. The first invasive fungal stages (germlings) were observed 8–12 hpi, and mycelium began to form in the soft tissue at approximately 12–16 hpi (Figures 2A–2C; Figures S2F and S2G), indicating rapid spread of the invasive *Rhizopus* infection throughout the tissue, consistent with the known explosive nature of this infection in susceptible human individuals (Farmakiotis and Kontoyiannis, 2016). Induced mucosal damage resulted in a significant increase in the number of adherent spores and the number of hyphal invasion sites per larva (Figure 2D), suggesting a morphological switch to a filamentous (hyphal) growth form associated with increased invasive disease (Lee et al., 2015).

Author Manuscript Author Manuscript Author Manuscript Author Manuscript

We next focused on exploration of early events governing impaired epithelial turnover and fungal adhesion to damaged epithelium. *In vivo* time-lapse imaging revealed loss of individual epithelial cells by extrusion, a process by which neighboring cells eject damaged cells from the tissue and seal the remaining gap to sustain barrier function and tissue integrity (Eisenhoffer et al., 2012; Lubkov and Bar-Sagi, 2014; Rosenblatt et al., 2001; Teo et al., 2020; Figures 2E–2G; Figures S3A–S3D; Videos S1 and S2). Importantly, we found that continual loss of multiple cells from tissue by extrusion results in elongation of neighboring cells and eventual loss of cell-cell contacts. Loss of cell-cell contacts because of increased cell extrusion presented as transient tears in the tissue (Figure 2F) and, eventually, large gaps between the surface epithelial cells (Figures 2H and 2I). Scanning electron microscopy further confirmed an affinity of invading fungi toward sites of epithelial injury with visibly impaired cell-cell junctions (Figures 2J and 2K). Consistent with the idea that repair of the injured mucosa is crucial for protection against fungal invasion, infection with *Rhizopus* following a brief recovery period from induced cell loss when there are little to no tears or gaps in the epithelial tissue led to significantly reduced infection-associated mortality (Figure 2L). Further, in contrast to elimination of surface cells by extrusion, no increase in mortality because of *R. arrhizus* infection was found after NTR/MTZ-induced damage to the basal stem cell population (Figure S3E). In this context, apoptotic cells become trapped between the basal and periderm layers and create bulges in the surface epithelium, but barrier function is not comprised (Brock et al., 2019; Eisenhoffer et al., 2017). These data establish a direct correlation between excessive epithelial cell extrusion leading to impaired integrity of intercellular junctions and lethal fungal invasion.

Adherence of fungal spores to damaged epithelia promotes hyphal growth

Epithelial damage can expose extracellular matrix proteins that provide focused points of interaction for inhaled, ingested, or encountered fungal spores (Baldin and Ibrahim, 2017; Watkins et al., 2018). We next examined the localization of different components of the extracellular matrix after induced epithelial cell extrusion and found increased exposure of laminin at sites of tissue damage. Adhered fungal spores were frequently located at sites of epithelial tissue damage that had exposed laminin (Figures 3A and 3B; Figure S4A). We also performed an *in vitro* spore adhesion assay to mimic the larval culture setting (E3 medium, 28°C) and observed increased *R. arrhizus* spore adhesion in well plates coated with increasing concentrations (0.1–5 μg/cm^2) of human laminin (Figure 3C) or fibronectin (Figure S4B), adhesion molecules that anchor cells to collagen or proteoglycan substrates (Pankov and Yamada, 2002; Bouchara et al., 1996). Furthermore, increased hyphal invasion was observed in areas of epithelial cell loss and tissue damage (Figures 3D and 3E; Video S3). These data suggest that contact of the *R. arrhizus* cell wall with the extracellular matrix component laminin contributed to adhesion. Therefore, we reasoned that pre-coating of the spores with laminin (Vicentini et al., 1994) may disrupt this interaction and block invasive infection. Indeed, incubation of the *R. arrhizus* spores with laminin (2 μg/mL) prior to infection significantly reduced mortality in larvae with induced cell loss (Figure 3F), whereas pre-coating with laminin did not interfere with fungal growth and morphogenesis *in vitro* (data not shown). We conclude from these data that transient tissue disintegrity caused by rapid extrusion of multiple epithelial cells exposes extracellular matrix components that facilitate establishment of substantial invasive mucormycosis.

Author Manuscript Author Manuscript Author Manuscript Author Manuscript

Adherence and hypha formation is a prerequisite for fungal invasion and mortality (Gebremariam et al., 2014); therefore, we next sought to determine whether previously associated virulence factors specific for Mucorales (Hassan and Voigt, 2019) contribute to invasive disease in our model. As proof of principle, we studied the virulence of *Rhizopus* with loss of the spore coat protein CotH (Gebremariam et al., 2014). CotH plays a key role as an invasin in the pathogenesis of mucormycosis (Gebremariam et al., 2014) and is detected universally on the spore surface of all Mucorales but not on other species (Hassan and Voigt, 2019). We found that loss of the spore coat protein CotH significantly attenuated the virulence of *Rhizopus* (Figure 3G), supporting the theory that CotH plays a key role as an invasin in the pathogenesis of opportunistic mucormycosis in our model. Although we observed no change in the ability of CotH RNAi spores to adhere to extracellular matrix (ECM) compounds *in vitro* (Figure S4C), zebrafish larvae express a homolog of the well-described epithelial CotH target GRP78 (Gebremariam et al., 2014; Liu et al., 2010; Thakur et al., 2014). Because translocation and dissemination by *C. albicans* has also been shown to be dependent on the ability to transform to the hyphal form (Koh et al., 2008), we next tested *C. albicans* mutants with deletions in genes involved in formation of pseudohyphae and hyphae (the transcription factors CPH1 and EFG1) (Lo et al., 1997, 2015). Compared with the isogenic wild type, infection with *cph1*-, *efg1*-, and *cph1/efg1*-deficient *C. albicans* mutants resulted in significantly decreased mortality (Figure 3H), suggesting that fungal virulence factors associated with adhesion and hyphal filamentation promote invasion in our mucosal injury model.

We then turned our attention to mitigation strategies to counteract fungal invasion in the setting of compromised epithelial integrity by exploring whether treatment with antifungal agents used in a clinical setting (posaconazole and amphotericin B) (Böhme et al., 2003; Greenberg et al., 2004; Vehreschild et al., 2013) could attenuate mortality in infected larvae with epithelial tissue damage (Figure 3I). Normalized to the number of larvae alive at the time of treatment, addition of amphotericin B (5 μg/mL) or posaconazole (5 μg/mL) to the larval culture medium improved 72-h survival rates from 55% to 82% ($p < 0.001$) and 88% ($p = 0.004$), respectively (Figure 3I). In contrast, exposure to voriconazole (with 5 μg/mL), an antifungal agent with no activity against *Rhizopus*, did not significantly alter survival rates (Figure 3I). Toxicity controls in the wild type and larvae with mucosal damage consistently revealed more than 90% 72-h survival rates after treatment with the three agents. In addition to enhancement of survival after infection, amphotericin B and posaconazole treatment significantly lowered *R. arrhizus* gene copy numbers (Figure S4C), further supporting the utility of our model as a platform to study the antifungal effects of known and unknown compounds in the context of mucosal injury and fungal infection.

Treatment with recombinant human EPGN (rhEPGN) suppresses epithelial cell extrusion and attenuates fungal invasion

We next explored strategies of enhancing mucosal barrier function as an important mechanism of action to mitigate invasive fungal infections. Larval zebrafish do not normally succumb to induced cell loss and compromised tissue integrity (Figure 1J; Figure S1G), suggesting that robust cell and molecular epithelial repair mechanisms rapidly restore barrier function. To identify the molecular events driving the observed host defense

Author Manuscript Author Manuscript Author Manuscript Author Manuscript

responses to mucosal damage, we performed RNA sequencing on whole larvae after induced epithelial cell loss (Figures 4A and 4B; NIH Gene Expression Omnibus: GSE1408392). Multiple pairwise comparison analysis and unsupervised hierarchical clustering (Figure 4A) identified 583 genes with unique differential expression during induced epithelial cell loss by extrusion (5 h) ($q < 0.05$, adjusted p value, DeSeq2 and Benjamini-Hochberg method for false discovery rate [FDR] correction, three independent biological replicates, 15–30 larvae per replicate; Table S1).

Gene Ontology (GO) biological process categorization suggested that the identified differentially expressed genes were involved in leukocyte migration (4.43e-3), response to stress (4.29e-3) and fatty acid biosynthesis (3.27e-3), and regulation of molecular function (1.62e-3) (Figure 4B). These leukocyte migration GO category contained genes involved in matrix metalloproteinase activity (*mmp9* and *mmp13a*) and cytokines (*il1b* and *cxcl8b*) involved in neutrophil recruitment (Altmeier et al., 2016; Xu et al., 2018), and the molecular function category included genes involved in epithelial growth factor signaling (*epigen*) (Kochupurakkal et al., 2005) and maintenance of tight junctions to sustain tissue integrity (*claudinB*) (Chelakkot et al., 2018; Kwong and Perry, 2013; Turksen and Troy, 2004).
To validate changes in target gene expression and also provide key information about its localization in tissue, we used *in situ* hybridization chain reaction (HCR), which enables high contrast and subcellular resolution to map target mRNAs within their native *in vivo* environment (Choi et al., 2018). We found significantly increased expression in *epigen* (Figure 4C), *mmp13a*, *il1b*, and *cxcl8b* (Figure S5A), at sites of epithelial cell loss in the tail fin epithelium. In contrast, increased EPGN expression was not observed after induced damage to the basal stem cell population (Figure S5B), a condition that did not increase mortality after *R. arrhizus* infection (Figure S3E). This dataset now provides a list of endogenous pathways that can potentially be targeted to enhance epithelial barrier function, guide neutrophil activity, and mitigate opportunistic fungal infection.

Our data pointed out an early role of the epidermal growth factor signaling ligand EPGN during induced cell extrusion (Figures 4A–4C). Combined with the known roles of EPGN (Kochupurakkal et al., 2005; Strachan et al., 2001) and the epidermal growth factor (EGF) signaling pathway in epithelial proliferation and cell elimination (Blay and Brown, 1985; Frey et al., 2006; Miguel et al., 2017; Moreno et al., 2019; Polk, 1998), these results suggest that transient increases in EPGN may aid in sustaining or re-establishing barrier function (Figure 4C). Therefore, we hypothesized that treatment with recombinant human EPGN (rhEPGN) could provide protective effects against epithelial tissue damage and prevent *R. arrhizus*-associated mortality. Addition of rhEPGN (250 nM) during MTZ-induced damage improved overall tissue morphology (Figure S5E), significantly increased 72-h survival rates from 47% to 88%(Figure 4D; $p < 0.001$), and alsoresulted in a reduced overall fungalburden per larva (Figure S5C). Importantly, we found that the time of addition of rhEPGN in relation to mucosal tissue damage was essential. Prophylactic treatment with rhEPGN marginally improved survival, whereas treatment during damage and infection provided significant benefit (Figure 4D). Similarly, treatment with recombinant human EGF (rhEGF) during damage and *Rhizopus* infection attenuated epithelial damage (Figures S5D and S5E) and significantly improved survival from 47% to 70% ($p < 0.003$). We conclude from these

Author Manuscript Author Manuscript Author Manuscript Author Manuscript

results that treatment with rhEGPN or rhEGF during induced epithelial cell extrusion and mucosal damage attenuates opportunisitic fungal invasion.

To directly test how EGF signaling could provide protective effects against opportunistic fungal invasion, we examined the downstream effectors of the EGF signaling pathway and the epithelial cell response to damage over time after treatment with rhEPGN. Inhibition of the EGF receptor (EGFR; pharmacological inhibitor AG1478) or of the downstream mitogen-activated protein kinase (MAPK) ERK 1/2 (MEK; pharmacological inhibitor U0126) in combination with rhEPGN treatment during damage and *Rhizopus* infection alleviated the observed protective effects and resulted in significantly worse overall survival (Figures 4E and 4F; Figure S5D). Intriguingly, we found that treatment with rhEPGN or rhEGF during MTZ treatment to induce mucosal damage prevented extrusion of NTR-positive epithelial cells and resulted in lack of mucosal tissue damage over the course of 5 h (Figures 4G–4K; Videos S4, S5, S6, and S7; Figure S5D). Hallmarks of extrusion (Eisenhoffer et al., 2012; Rosenblatt et al., 2001), including cell rounding and accumulation of F-actin at the cortex (Figures S3A–S3D), were absent from rhEPGN- and rhEGF-treated larvae. Brief rhEPGN treatment during damage did not enhance stem cell proliferation, which remained proportional to the amount of damage sustained (Figure S6A). We next sought to test whether suppressing extrusion independent of EGF signaling could also mitigate opportunistic infection. Cells in the process of extrusion produce sphingosine-1-phosphate (S1P), which binds to the $S1P_2$ receptor in neighboring cells to trigger actomyosin contraction and expulsion of the unfit cell (Gu et al., 2011). Blocking extrusion via inhibition of sphingosine kinase 1 (SKI5C) in combination with MTZ-induced damage and infection also significantly increased 72-h survival rates from 47% to 65% (Figure S6B; $p < 0.021$). We conclude that treatment with EPGN and EGF suppresses epithelial cell extrusion through a MEK-ERK signaling mechanism to prevent decreased integrity and provide protective effects against opportunistic infection.

The epithelium works in concert with immune cells to sense and respond to fungal pathogens and other noxious stimuli, and neutrophils are one of the first defenders of innate immune response against tissue injury and infection (Amulic et al., 2012; Cvejic et al., 2008; Poplimont et al., 2020; Schoen et al., 2019; Wang, 2018). Our data also suggested that epithelial cell loss stimulates production of chemoattractants for recruitment of neutrophils to sites of mucosal damage (Figures 4A and 4B; Figure S5A). Therefore, we next sought to define the response of neutrophils after induced cell loss and infection with *R. arrhizus*. We observed a significant increase in the number of neutrophils present in the epithelium during mucosal damage associated with cell loss and cell loss-mediated opportunisitic infection with *R. arrhizus*, suggesting that neutrophils are attracted to sites of presumptive damage and infection (Figures 5A–5D). We used *in vivo* time-lapse imaging to track neutrophil dynamics over time and found that induced cell loss promoted increased numbers of neutrophils with behaviors consistent with exploratory patrolling behavior (Poplimont et al., 2020) within the epithelial tissue (Figures 5E–5H). Moreover, neutrophils have been observed undergoing directed migration (Barros-Becker et al., 2017) to sites of extrusion (Figure 5I) as well as to sites of epithelial damage and *R. arrhizus* infection (Figure S6C). Suppressing extrusion by treatment with rhEPGN resulted in reduced numbers of circulating neutrophils (Figure 5H) and a decrease in expression of the epithelial cell loss-induced

Author Manuscript Author Manuscript Author Manuscript Author Manuscript

neutrophil-attracting chemokines *mmp13a* and *il1b* (Figures 5J and 5K). These data suggest that epithelial cell loss promotes recruitment of neutrophils to sites with breaches in mucosal tissue and areas of potential opportunisitic fungal infection.

DISCUSSION

Establishment of a mucosal damage-mediated infection model in larval zebrafish allowed us to define some of the earliest events of opportunistic fungal pathogenesis in living epithelia. Unlike previous zebrafish mucormycosis studies that circumvented mucosal invasion by direct injection of spores into the hindbrain ventricle or swim bladder (López-Muñoz et al., 2018; Tatara et al., 2018; Voelz et al., 2015), our approach is more pathogenetically similar to fungal infections in humans, which are often associated with disrupted epithelial homeostasis and compromised integrity following trauma or exposure to cytotoxic chemotherapy (Jacobsen, 2019; Walsh et al., 2019). Using this model, we demonstrate how extrusion of numerous epithelial cells from the tissue can expose underlying ECM components to promote increased attachment and invasion into surrounding tissues of fungi associated with human disease.

Many human fungal pathogens associated with the respiratory, gastrointestinal, or urogenital tracts have the capacity to bind proteins that comprise the ECM (Bouchara et al., 1996; Singh et al., 2012), and loss of epithelial integrity can promote increased levels of these ECM components (Gago et al., 2018). Thus, exposed ECM may serve to enhance adhesion of fungi to damaged mucosae and facilitate spread of infection to deeper tissues (Singh et al., 2012). In support of this, our data show that mucosal damage and the subsequent exposure of laminin resulted in a significant increase in the number of adherent spores, hypha formation in areas with compromised integrity, and invasive disease. Importantly, our data suggest that disrupting the ability of fungi to interact with laminin may provide protective effects against opportunistic infection.

By interrogating how excessive cell loss disrupts homeostasis and promotes opportunistic fungal infection, we identified extrusion as a key homeostatic mechanism that can be manipulated to aid in sustaining barrier function and mitigating subsequent invasion. Mucosal damage caused by extrusion of numerous cells stimulates production of *epigen*, *mmp13a*, and *il1b*, genes involved in epithelial repair (Coleman et al., 2015; Kochupurakkal et al., 2005; Xu et al., 2018; Yoshinari et al., 2009) and recruitment of neutrophils (Altmeier et al., 2016; Voelz et al., 2015) to sites of injury or infection. Our data show that treatment with rhEPGN suppresses extrusion through MEK-ERK signaling to prevent tissue disintegrity in the face of damage, leading to decreased opportunistic infection and improvement of overall survival. Additionally, fungal infection might also activate EGF pathways. For instance, *C. albicans* and its associated secreted toxin candidalysin, can induce shedding of EGF ligands, including EPGN, to trigger EGFR activation and signaling, modulating early epithelial and immune cell responses during infection (Ho et al., 2019). Thus, both mechanisms could be operating at sites of mucosal breach and opportunistic fungal infection *in vivo*, supporting the idea of pathogen exploitation of the EGFR pathway and host-protective functions occurring in parallel (Ho et al., 2019).

Author Manuscript Author Manuscript Author Manuscript Author Manuscript

Our study provides insights into how disruption of mucosal homeostasis promotes a switch from commensal organism to invasive fungal pathogen. This *in vivo* platform now provides the opportunity to rapidly test exogenous factors that may stimulate epithelial restoration mechanisms and/or modulate the immune system to attenuate fungal invasion in the setting of mucositis. Leveraging endogenous pathways via addition of exogenous factors to protect against epithelial damage or enhance the rate of epithelial repair could result in an additional area of therapeutic treatment options to reduce susceptibility to infection.

STAR★METHODS

Detailed methods are provided in the online version of this paper and include the following:

RESOURCE AVAILABILITY

Lead contact—Further information and request for resources and reagents should be directed to and will be fulfilled by the Lead Contact, George Eisenhoffer (gteisenhoffer@mdanderson.org).

Materials availability—Transgenic zebrafish lines used in this study are available upon request.

Data and code availability—The RNaseq dataset generated during this study is available at the NCBI Expression Omnibus (GEO: GSE140839).

EXPERIMENTAL MODEL AND SUBJECT DETAILS

Zebrafish—Zebrafish were maintained under standard laboratory conditions with a cycle of 14 h of light and 10 h of darkness. Embryos were collected and kept in E3 embryo medium at 28.5 C and staged as described in Kimmel et al. (1995). The zebrafish used in this study were handled in accordance with the guidelines of the University of Texas MD Anderson Cancer Center Institutional Animal Care and Use Committee. The following zebrafish strains were used: *Et(Gal4-VP16)*^{zc1044}*;Tg(UAS-1b:nsfB-mCherry)*^{c264,} (Davison et al., 2007; Eisenhoffer et al., 2017), *Et(Gal4-VP16)*^{zc1044}*;Tg(UAS-1b:nsfB-mCherry)*^{c264}*;Tg(UAS-1b:Lifeact-EGFP)*^{utm1,} (Eisenhoffer et al., 2017; Franco et al., 2019), *Et(Gal4-VP16)*^{zc1036A}*;Tg(UAS-1b:nsfB-mCherry)*^{c264,} (Eisenhoffer et al., 2017), *Tg(krt4:GFP)* (Gong et al., 2002), *Tg(−8.0cldnb:lynEGFP)* ^{zf106,} (Haas and Gilmour, 2006) and *Tg(mpo::GFP)* (Renshaw et al., 2006).

Fungal Strains—Clinical isolates of *Rhizopus arrhizus* (#749), *Mucor circinelloides* (#518), and *Candida albicans* (Y4215) were obtained from patients at the University of Texas MD Anderson Cancer Center. In addition, the following fungal mutants were used: FTR1-GFP-*R. arrhizus*, CotH RNAi *R. arrhizus*, and the isogenic empty RNAi control *R. arrhizus* strain (kind gifts from Dr. A. S. Ibrahim, University of California, Los Angeles) as well as efg1$^{-/-}$ *C. albicans*, cph1$^{-/-}$ *C. albicans*, efg1$^{-/-}$ cph1$^{-/-}$ *C. albicans*, and the isogenic *C. albicans* strain SC5314 (kind gifts from Dr. J. L. Lopez-Ribot, The University of Texas at San Antonio).

Author Manuscript Author Manuscript Author Manuscript Author Manuscript

Clinical Mucorales isolates were grown on yeast extract agar medium (YAG) for 48–72 h at 37°C. The *R. arrhizus* mutants were kept on YNB +csm (complete supplement mixture) -uracil medium for 3–5 days. Spores were collected in E3 by gently scraping the mycelium with a sterile glass rod.

All *Candida* isolates were streaked on Yeast Peptone Dextrose Agar (YPD) plates for single colony isolation. Single colonies were then grown in 5 mL of YPD liquid medium overnight at 35°C. On the following day, 100 mL of the overnight cultures were added to 5 mL of fresh YPD liquid medium and grown to mid-log phase. All fungal suspensions were washed twice with sterile E3 and spore concentrations were determined using a hemocytometer.

METHOD DETAILS

Metronidazole exposure, infection, and antifungal treatment of zebrafish larvae—The GAL4 enhancer trap lines *Et(Gal4-VP16)*^{zc1044A} and *Et(Gal4-VP16)*^{zc1036A} (Eisenhoffer et al., 2017) were used to drive the expression of *Tg(UAS-1b:nsfB-mCherry)*^{c264} (Davison et al., 2007) in either the outermost layer or basal layer of the epithelium in zebrafish embryos. Day 4 post fertilization (dpf) larvae were placed in 12-well plates, each well containing 10–15 larvae in 1 mL of E3 medium, using sterile 3-mL plastic transfer pipettes. Unless indicated otherwise, metronidazole (MTZ, Sigma Aldrich Product: M3761) was added to each well to a final concentration of 10 mM and incubated for 5 h. Subsequently, all wells were washed three times with fresh E3 to remove any residual MTZ. Next, 1 mL of fungal spore solution (dissolved in E3) or plain E3 medium was added for 16 h. After this period of fungal exposure, larvae were washed with fresh E3 and allowed to recover. During this recovery period larvae were allowed to recover either in plain E3 or E3 which was supplemented with antifungal agents for drug treatment cohorts. Survival of all larvae was monitored daily for 72 h post-infection (7 dpf). Dead or moribund larvae (no swimming motions after gentle probing with a 3-mL transfer pipette and/or absence of heart pulsation) were removed at 16, 24 and 48 h post-infection. All incubation steps were performed at 28°C on a nutator. At the end of the observation period, remaining larvae were humanely euthanized by placing them in ice water for 20 min.

Chemical Inhibitors and Recombinant Growth Factors—Larvae were treated with either 30 nM rhEGF (Prospec Protein Specialists Product: CYT-217-b) or 250 nM rhEPGN (Peptides International Product: CYT-601) for a 24-h period prior to, during or immediately after 5 h MTZ (10 mM) treatment. Chemical inhibitor assays were conducted using the same protocol in the presence or absence of either 5 μM of the EGF receptor inhibitor AG1478 (EMD Millipore Product: 658552) or 50 μM of the MEK inhibitor U0126 (MD Millipore Product: 662005).

Antifungals—The following antifungal agents were used: Posaconazole (Toronto Research Chemicals Product: P689600), voriconazole (Sigma-Aldrich Product: 32483), and amphotericin B (Sigma-Aldrich Product: 46006). All antifungals were freshly dissolved in E3 medium on the day of use. Antifungals were added to the larvae at a final concentration of 5 μg/mL at 16 h post-infection (after the wash step).

Author Manuscript Author Manuscript Author Manuscript Author Manuscript

Laminin coating of fungus before infection—*Rhizopus arrhizus* (#749) spores were harvested, counted, and suspended in E3 as described above (5×10^7/mL). Thereafter, 1-mL aliquots of the spore suspension were supplemented or not with 0.2 μg/mL or 2 μg/mL recombinant human laminin 521 (Thermo Fisher, A29249) and incubated on the nutator for 2 h at 28°C. Spores were then washed twice with sterile E3 and suspended at 5×10^7 spores per mL E3. Infection of MTZ-treated *Et(Gal4-VP16)*^{zc1044A}*;Tg(UAS-1b:nsfB-mCherry)*^{c264} larvae with 5×10^6 spores per mL (final concentration), washing at 16 h post-infection, and survival monitoring for 72 h were performed as described above.

***In vitro* fungal growth assay on extracellular matrix-component coated plates—**96-well flat bottom plates were coated with 0–5 μg/cm^2 laminin (Sigma Aldrich Product: AG56P) or fibronectin (Sigma-Aldrich Product: F0895) for 2 h at room temperature. Thereafter, plates were washed with E3 medium and 1000 spores of *R. arrhizus* (clinical isolate #749, CotH RNAi, or Control RNAi), suspended in 100 μL E3 medium, were added to each well. After overnight incubation (16 h) on the nutator at 28°C, wells were carefully washed twice with fresh E3 medium to remove non-adherent spores. The number of remaining (adherent) spores was then quantified using the IncuCyte ZOOM microscopy platform and its Basic Analyzer module in combination with previously developed detection algorithms (Wurster et al., 2019). Four wells were tested for each extracellular matrix compound and concentration.

Determination of fungal burden by 18S qPCR—Dead larvae were collected at 16, 24, 48, and 72 h post-infection, washed three times with cold E3, and frozen in 0.5 mL E3 at −80°C. Remaining (surviving) larvae were humanely euthanized in ice-cold E3 at 72 h post-infection, washed, and frozen in 0.5 mL E3 at −80°C. Samples from the same experimental cohort, collected at different time points, were combined, washed, and homogenized in 2 mL cold E3 using a 2-mL screw-cap cryovial containing acid-washed glass beads. Tissue was then homogenized in alternating 15 s bursts in a mini bead beater (Bio-Spec, Bartlesville, OK) followed by cooling in crushed ice. DNA was then isolated from an aliquot of the larval homogenate (80 μL) using the DNeasy kit (QIAGEN Product: 69506) and analyzed in triplicate by real-time quantitative PCR (qPCR) using primers and dually labeled hybridization probes specific for *R. arrhizus* 18S rRNA genes as previously described (Ibrahim et al., 2005). The cycle threshold of each sample was interpolated from a seven-point standard curve prepared by spiking uninfected larvae with known concentrations of strain *R. arrhizus* #749 (10^2 to 10^8 spores/mL larval homogenate).

Immunohistochemistry—Zebrafish larvae were fixed by overnight rocking in a fixative solution of 4% paraformaldehyde in phosphate buffered saline (PBS) with 0.05% Triton X-100 (PBSTX) at 4°C. Larvae were then washed with PBSTX x 0.05% and blocked for 1 h at room temperature with a PBSTX x 0.05% solution supplemented with 1% DMSO and 2 mg/mL bovine serum albumin (BSA) blocking solution. Larvae were incubated overnight at 4°C with primary antibody diluted in blocking solution. Larvae were washed (PBSTX x 0.05%) and incubated overnight at 4°C with secondary antibody diluted in blocking solution. Finally, larvae were washed (PBSTX x 0.05%) and mounted for imaging.

Author Manuscript Author Manuscript Author Manuscript Author Manuscript

Primary Antibodies and Dyes—Activate caspase-3 (BD Biosciences Product: 559565, 1:700); BrdU (Abcam Product: ab6326, 1:100); Tp63 (Genetex Product: GTX124660, 1:500); Laminin (Sigma Product: L9393); DAPI (ThermoFisher Product: D1306, 1:1000)

Laminin Staining—Larvae were fixed, delicately washed twice with PBSTX x 0.5%, left in blocking buffer on benchtop for 2 h, placed in primary antibody, and incubated in a 4°C cold room on shelf for 2 days. Primary antibody was then removed, larvae were delicately washed with PBSTX x 0.5% three times, blocking buffer was added and larvae were incubated on benchtop for 2 h. Thereafter, blocking buffer was removed and larvae were incubated with secondary antibody overnight at 4°C without rocking. The following day, the secondary antibody was removed, the larvae were delicately washed 3 times with PBSTX x 0.5%, and incubated on benchtop in DAPI (Thermo Fisher Product: D1306) diluted at 1:1000 for 45 min. Finally, the larvae were delicately washed 3 times in PBSTX x 0.5%, transferred to 1 x PBS and mounted for imaging.

Confocal Microscopy—Live imaging experiments were performed by first anesthetising zebrafish larvae with 0.04% Tricaine-S (Western Chemical: TRICMGR0100) in E3. Anesthetised larvae were then mounted on a 35-mm MatTek glass bottom dish (MatTek Product: P35G-1.0–20-C) with 1% low melt agarose (Invitrogen Product: 16520). All live imaging experiments involving live fungus were imaged with an Olympus Fluoview FV3000 laser scanning confocal microscope by using the supplied Olympus Fluoview Acquisiton FV31S-SW software. All other confocal imaging experiments were acquired on a Zeiss LSM800 laser scanning microscope.

Scanning electron microscopy—Samples were fixed in 3% glutaraldehyde + 2% paraformaldehyde in 0.1 M cacodylate buffer (pH 7.3). Samples were washed with 0.1 M cacodylate buffer (pH 7.3), post-fixed with 1% cacodylate buffered osmium tetroxide, washed with 0.1 M cacodylate buffer and then with distilled water. Samples were treated with Millipore-filtered 1% aqueous tannic acid, washed in distilled water, treated with Millipore-filtered 1% aqueous uranyl acetate and then rinsed with distilled water. They were dehydrated with a series of increasing concentrations of ethanol and transferred to increasing concentrations of hexamethyldisilazane. After overnight air-drying, samples were mounted onto double-stick carbon tabs (Ted Pella. Inc., Redding, CA), and mounted onto glass microscope slides. Samples were coated under vacuum using a Balzer MED 010 evaporator (Technotrade International, Manchester, NH) with platinum alloy for a thickness of 25 nm and then flash carbon coated under vacuum. Samples were then transferred to a desiccator until examination and imaging in a JSM-5910 scanning electron microscope (JEOL, USA, Inc., Peabody, MA) at an accelerating voltage of 5 kV.

Live imaging in the IncuCyte ZOOM time-lapse microscopy system—4 dpf *Et(Gal4-VP16)*^{zc1044A}*;Tg(UAS-1b:nsfB-mCherry)*^{c264} larvae were treated with MTZ (10 mM, 5 h) and washed in 12-well plates as described above. Larvae were then anesthetized with tricaine, placed in the middle of each well of a 24-well flat bottom plate, and mounted with a drop of low melting agarose under a stereomicroscope. The wells were infected with 500 µL E3 containing 5 × 10^6/mL FTR1-GFP-*R. arrhizus* spores. Imaging was performed at

Author Manuscript Author Manuscript Author Manuscript Author Manuscript

28°C in the IncuCyte ZOOM HD/2CLR time lapse microscopy system (Sartorius) equipped with an IncuCyte ZOOM 10 x PLAN FLUOR objective (Sartorius). Phase contrast, red (800 ms) and green (400 ms) fluorescence channels were imaged every 3 hours. 36 frames were captured per well. The Basic Analyzer image analysis tool was used to track and quantify fungal growth in the larval tissue. The algorithm was optimized using a training image collection as previously described (Wurster et al., 2019). The GFP-positive area was quantified both absolutely (in μm^2) and in relation to the red fluorescent area (%). To create time lapse movies, stacks of images were exported in tagged image file format(tif) using the Time Plot function in the IncuCyte ZOOM software. Videos were assembled and annotated in Microsoft PowerPoint, and exported in MP4 format.

Fin Area Measurements—Zen 2.6 (blue edition) was used to perform fin area measurements. A straight line was drawn perpendicular to the tip of the notochord and the contour (polygon) tool was used to trace the outline of the fin. The fin area measurements were then sorted into three categories. Class 0 was designated as fin area greater than 60000 μm^2, Class 1 was designated as fin area between 40000 and 60000 μm^2, and Class 2 was designated as less than 40000 μm^2. Three independent replicates were performed. The total number of each designated rank for each condition was then plotted on a contingency graph in GraphPad Prism 7.03.

Whole-mount zebrafish RNA *in situ* hybridization—RNA *in situ* detection was achieved by using hybridization chain reaction version 3.0 (HCR v3.0) reagents from Molecular Instruments (Choi et al., 2018). The GAL4 enhancer trap lines *Et(Gal4-VP16)*^{zc1044A} and *Et(Gal4-VP16)*^{zc1036A} (Eisenhoffer et al., 2017) were used to drive the expression of *Tg(UAS-1b:nsfB-mCherry)*^{c264} in either the outermost layer or basal layer of the epithelium in zebrafish embryos. On day 4 post-fertilization, 10 to 15 larvae were treated with 10 mM MTZ (Sigma Aldrich Product: M3761) for 5 h and washed in 6-well plates as described above. Zebrafish larvae were then placed into Eppendorf tubes and fixed by overnight rocking in a fixative solution of 4% paraformaldehyde in phosphate buffered saline (PBS) with 0.1% Tween-20 (Sigma Aldrich Product: P9416–100mL) at 4°C. Larvae were then rinsed twice with PBS. Thereafter, larvae were rinsed twice in PBS-Tween 0.1% and then rocked twice for 5 min each in 0.1% PBS-Tween-20. The larvae were then transferred to new Eppendorf tubes with 500 µL of pre-warmed probe hybridization buffer (Molecular Instruments Product: whole-mount probe hybridization buffer) and rocked for 30 min at 37°C. The probe solution was prepared by adding 2 pmol of each specific probe (Molecular Instruments Product: HCR v3.0 custom probe) to 500 µL of pre-warmed probe hybridization buffer. Next, probe hybridization buffer was removed and samples were incubated in 500 µL of freshly-made probe solution and rocked overnight at 37°C. Samples were then washed 4 times for 15 minutes each with 750 µL of pre-warmed probe wash buffer (Molecular Instruments Product: whole-mount probe wash buffer) to remove excess probe. Larvae were then washed twice for 5 min each with 5X-SSC-0.1% Tween-20 (Sigma Aldrich Product: S6639) at room temperature. Next, larvae were pre-amplified with 500 µL of amplification buffer (Molecular Instruments Product: whole-mount amplification buffer) for 30 min a room temperature. Metastable hairpins were prepared by snap-cooling 10 µL of3 µM of h1 (Molecular Instruments Product: HCR v3.0 Amplifier) and h2 (Molecular

Author Manuscript Author Manuscript Author Manuscript Author Manuscript

Instruments Product: HCR v3.0 Amplifier) stocks at 95°C for 90 s and then allowed to cool in a dark drawer for 30 min. After cooling, h1 and h2 hairpins were added to 500 μL of amplification buffer at room temperature. Larvae were then removed from pre-amplification solution and placed in hairpin solution and rocked for 18 h in the dark at room temperature. Finally, excess hairpin solution was removed with the following series of washes using 5X-SSCT at room temperature; 2× 5 min, 2× 30 min and 1× 5 min. To ensure that all samples were flat as possible and to ensure that tissue morphology was maintained, samples were mounted on MatTek dishes using low melt agarose and imaged using a Zeiss LSM-800 confocal microscope as described above.

RNA sequencing—RNA sequencing was performed on whole larvae under homeostatic conditions (no MTZ), and 5 h after induced epithelial cell loss by addition of MTZ (Gene Expression Omnibus accession # GSE140839). For each time point and condition analyzed, 15 to 30 individual zebrafish larvae were pooled and placed in Trizol for subsequent RNA extraction. The RNeasy kit (QIAGEN Cat. No. 74104) was used to extract total RNA with an additional on-column RNase-free DNase (QIAGEN Cat No: 79254) treatment. Samples were prepared in triplicate and sequenced across multiple lanes using a the TrueSeq Stranded Total RNA-seq kit on a HiSeq 4000 instrument.

Bioinformatics Methods—FastQC version 0.11.8 was used as an initial quality control check for all samples. Trimmomatic version 0.33 (Bolger et al., 2014) was then used to remove adaptor sequences and trim reads. All reads were then aligned to the Zebrafish genome version GRCz11(NCBI Genebank: GCA_000002035.4) using HiSat2 version 2.0.4 (Kim et al., 2019). The Samtools package version 1.8 (Li et al., 2009) was then used to convert, sort and index the reads. Finally, the Featurecounts program version1.6.3 (Liao et al., 2014) was used to generate a table of counts for each sample analyzed. The DeSeq2 package version 1.24 (Love et al., 2014) was run on R-Studio version 1.2.5033 (https://www.rstudio.com/) using R core version 3.6.0 (https://www.R-project.org/) to identify differentially expressed transcripts across samples. The GOEnrichment package, (https://github.com/DanFaria/GOEnrichment) was used to identify Gene Ontology categories enriched in each condition.

QUANTIFICATION AND STATISTICAL ANALYSIS

Data analysis was performed using Microsoft Excel 2013 and GraphPad Prism 7.03. Three to five independent replicates of each experiment were performed for survival analysis. Aggregated data and standard deviations are shown in the survival plots. Significance tests are specificied in the figure legends. Significance levels are denoted by asterisks: * $p < 0.05$, ** $p < 0.01$, *** $p < 0.001$.

Supplementary Material

Refer to Web version on PubMed Central for supplementary material.

Author Manuscript Author Manuscript Author Manuscript Author Manuscript

ACKNOWLEDGMENTS

This work was supported by the Cancer Prevention Institute of Texas (RR14007), the National Institute of General Medical Sciences (GM124043), and the Linda and Mark Quick Award for Basic Science (to G.T.E.) and in part by a Cancer Center support grant (P30CA016672), the Texas 4000 distinguished professorship endowment, and the Robert C. Hickey Chair in Clinical Care endowment (to D.P.K.). We thank Kenneth Dunner, Jr. at the UT MD Anderson High Resolution Electron Microscopy Facility for assistance with electron microscopy data and Jordan Pietz at the Creative Communications group at MD Anderson Cancer Center for biomedical visualization. The High Resolution Electron Microscopy and Flow Cytometry and Cellular Imaging core facilities were supported by CCSG grant NIH P30CA016672. The Sequencing and Microarray facility was supported by a National Cancer Institute grant (CA016672).

REFERENCES

Altmeier S, Toska A, Sparber F, Teijeira A, Halin C, and LeibundGut-Landmann S (2016). IL-1 Coordinates the Neutrophil Response to C. albicans in the Oral Mucosa. PLoS Pathog. 12, e1005882.

Amulic B, Cazalet C, Hayes GL, Metzler KD, and Zychlinsky A (2012). Neutrophil function: from mechanisms to disease. Annu. Rev. Immunol. 30, 459–489. [PubMed: 22224774]

Atieh Y, Wyatt T, Zaske AM, and Eisenhoffer GT (2020). Pulsatile contractions promote apoptotic cell extrusion in epithelial tissues. Curr. Biol, S0960–9822(20)31825-X.

Baldin C, and Ibrahim AS (2017). Molecular mechanisms of mucormycosis-The bitter and the sweet. PLoS Pathog. 13, e1006408.

Barros-Becker F, Lam PY, Fisher R, and Huttenlocher A (2017). Live imaging reveals distinct modes of neutrophil and macrophage migration within interstitial tissues. J. Cell Sci. 130, 3801–3808. [PubMed: 28972134]

Blay J, and Brown KD (1985). Epidermal growth factor promotes the chemotactic migration of cultured rat intestinal epithelial cells. J. Cell. Physiol. 124, 107–112. [PubMed: 3876338]

Böhme A, Ruhnke M, Buchheidt D, Karthaus M, Einsele H, Guth S, Heussel G, Heussel CP, Junghanss C, Kern WK, et al. ; Infectious Diseases Working Party (AGIHO) of the German Society of Hematology and Oncology (DGHO) (2003). Treatment of fungal infections in hematology and oncology–guidelines of the Infectious Diseases Working Party (AGIHO) of the German Society of Hematology and Oncology (DGHO). Ann. Hematol. 82 (Suppl 2), S133–S140. [PubMed: 13680170]

Bolger AM, Lohse M, and Usadel B (2014). Trimmomatic: a flexible trimmer for Illumina sequence data. Bioinformatics 30, 2114–2120. [PubMed: 24695404]

Bouchara JP, Oumeziane NA, Lissitzky JC, Larcher G, Tronchin G, and Chabasse D (1996). Attachment of spores of the human pathogenic fungus Rhizopus oryzae to extracellular matrix components. Eur. J. Cell Biol. 70, 76–83. [PubMed: 8738422]

Brock CK, Wallin ST, Ruiz OE, Samms KM, Mandal A, Sumner EA, and Eisenhoffer GT (2019). Stem cell proliferation is induced by apoptotic bodies from dying cells during epithelial tissue maintenance. Nat. Commun. 10, 1044. [PubMed: 30837472]

Chelakkot C, Ghim J, and Ryu SH (2018). Mechanisms regulating intestinal barrier integrity and its pathological implications. Exp. Mol. Med. 50, 1–9.

Chen YK, Hsue SS, and Lin LM (2005). Expression of p63 protein and mRNA in oral epithelial dysplasia. J. Oral Pathol. Med. 34, 232–239. [PubMed: 15752259]

Choi HMT, Schwarzkopf M, Fornace ME, Acharya A, Artavanis G, Stegmaier J, Cunha A, and Pierce NA (2018). Third-generation *in situ* hybridization chain reaction: multiplexed, quantitative, sensitive, versatile, robust. Development 145, dev165753.

Claudinot S, Sakabe JI, Oshima H, Gonneau C, Mitsiadis T, Littman D, Bonfanti P, Martens G, Nicolas M, Rochat A, and Barrandon Y (2020). Tp63-expressing adult epithelial stem cells cross lineages boundaries revealing latent hairy skin competence. Nat. Commun. 11, 5645. [PubMed: 33159086]

Coleman EA, Lee JY, Erickson SW, Goodwin JA, Sanathkumar N, Raj VR, Zhou D, McKelvey KD, Apewokin S, Stephens O, et al. (2015). GWAS of 972 autologous stem cell recipients

Author Manuscript Author Manuscript Author Manuscript Author Manuscript

with multiple myeloma identifies 11 genetic variants associated with chemotherapy-induced oral mucositis. Support. Care Cancer 23, 841–849. [PubMed: 25218607]

Curado S, Stainier DY, and Anderson RM (2008). Nitroreductase-mediated cell/tissue ablation in zebrafish: a spatially and temporally controlled ablation method with applications in developmental and regeneration studies. Nat. Protoc. 3, 948–954. [PubMed: 18536643]

Cvejic A, Hall C, Bak-Maier M, Flores MV, Crosier P, Redd MJ, and Martin P (2008). Analysis of WASp function during the wound inflammatory response–live-imaging studies in zebrafish larvae. J. Cell Sci. 121, 3196–3206. [PubMed: 18782862]

Dane PJ, and Tucker JB (1985). Modulation of epidermal cell shaping and extracellular matrix during caudal fin morphogenesis in the zebra fish Brachydanio rerio. J. Embryol. Exp. Morphol. 87, 145–161. [PubMed: 4031750]

Davison JM, Akitake CM, Goll MG, Rhee JM, Gosse N, Baier H, Halpern ME, Leach SD, and Parsons MJ (2007). Transactivation from Gal4-VP16 transgenic insertions for tissue-specific cell labeling and ablation in zebrafish. Dev. Biol. 304, 811–824. [PubMed: 17335798]

Eisenhoffer GT, Loftus PD, Yoshigi M, Otsuna H, Chien CB, Morcos PA, and Rosenblatt J (2012). Crowding induces live cell extrusion to maintain homeostatic cell numbers in epithelia. Nature 484, 546–549. [PubMed: 22504183]

Eisenhoffer GT, Slattum G, Ruiz OE, Otsuna H, Bryan CD, Lopez J, Wagner DS, Bonkowsky JL, Chien CB, Dorsky RI, and Rosenblatt J (2017). A toolbox to study epidermal cell types in zebrafish. J. Cell Sci. 130, 269–277. [PubMed: 27149923]

Farmakiotis D, and Kontoyiannis DP (2016). Mucormycoses. Infect. Dis. Clin. North Am. 30, 143–163.

Franco JJ, Atieh Y, Bryan CD, Kwan KM, and Eisenhoffer GT (2019). Cellular crowding influences extrusion and proliferation to facilitate epithelial tissue repair. Mol. Biol. Cell 30, 1890–1899. [PubMed: 30785842]

Frey MR, Dise RS, Edelblum KL, and Polk DB (2006). p38 kinase regulates epidermal growth factor receptor downregulation and cellular migration. EMBO J. 25, 5683–5692. [PubMed: 17139251]

Gago S, Overton NLD, Ben-Ghazzi N, Novak-Frazer L, Read ND, Denning DW, and Bowyer P (2018). Lung colonization by Aspergillus fumigatus is controlled by ZNF77. Nat. Commun. 9, 3835. [PubMed: 30237437]

Gebremariam T, Liu M, Luo G, Bruno V, Phan QT, Waring AJ, Edwards JE Jr., Filler SG, Yeaman MR, and Ibrahim AS (2014). CotH3 mediates fungal invasion of host cells during mucormycosis. J. Clin. Invest. 124, 237–250. [PubMed: 24355926]

Gong Z, Ju B, Wang X, He J, Wan H, Sudha PM, and Yan T (2002). Green fluorescent protein expression in germ-line transmitted transgenic zebrafish under a stratified epithelial promoter from keratin8. Dev. Dyn. 223, 204–215. [PubMed: 11836785]

Greenberg RN, Scott LJ, Vaughn HH, and Ribes JA (2004). Zygomycosis (mucormycosis): emerging clinical importance and new treatments. Curr. Opin. Infect. Dis. 17, 517–525. [PubMed: 15640705]

Gu Y, Forostyan T, Sabbadini R, and Rosenblatt J (2011). Epithelial cell extrusion requires the sphingosine-1-phosphate receptor 2 pathway. J. Cell Biol. 193, 667–676. [PubMed: 21555463]

Haas P, and Gilmour D (2006). Chemokine signaling mediates self-organizing tissue migration in the zebrafish lateral line. Dev. Cell 10, 673–680. [PubMed: 16678780]

Hassan MIA, and Voigt K (2019). Pathogenicity patterns of mucormycosis: epidemiology, interaction with immune cells and virulence factors. Med. Mycol. 57 (Supplement_2), S245–S256. [PubMed: 30816980]

Ho J, Yang X, Nikou SA, Kichik N, Donkin A, Ponde NO, Richardson JP, Gratacap RL, Archambault LS, Zwirner CP, et al. (2019). Candidalysin activates innate epithelial immune responses via epidermal growth factor receptor. Nat. Commun. 10, 2297. [PubMed: 31127085]

Hooper CE (1956). Cell turnover in epithelial populations. J. Histochem. Cytochem. 4, 531–540. [PubMed: 13385475]

Ibrahim AS, and Voelz K (2017). The mucormycete-host interface. Curr. Opin. Microbiol. 40, 40–45. [PubMed: 29107938]

Author Manuscript Author Manuscript Author Manuscript Author Manuscript

Ibrahim AS, Bowman JC, Avanessian V, Brown K, Spellberg B, Edwards JE Jr., and Douglas CM (2005). Caspofungin inhibits Rhizopus oryzae 1,3-beta-D-glucan synthase, lowers burden in brain measured by quantitative PCR, and improves survival at a low but not a high dose during murine disseminated zygomycosis. Antimicrob. Agents Chemother. 49, 721–727. [PubMed: 15673756]

Ibrahim AS, Gebremariam T, Lin L, Luo G, Husseiny MI, Skory CD, Fu Y, French SW, Edwards JE Jr., and Spellberg B (2010). The high affinity iron permease is a key virulence factor required for Rhizopus oryzae pathogenesis. Mol. Microbiol. 77, 587–604. 10.1111/j.1365-2958.2010.07234.x. [PubMed: 20545847]

Ibrahim AS, Spellberg B, Walsh TJ, and Kontoyiannis DP (2012). Pathogenesis of mucormycosis. Clin. Infect. Dis. 54 (Suppl 1), S16–S22. [PubMed: 22247441]

Jacobsen ID (2019). Animal Models to Study Mucormycosis. J. Fungi (Basel) 5, 27.

Kim D, Paggi JM, Park C, Bennett C, and Salzberg SL (2019). Graph-based genome alignment and genotyping with HISAT2 and HISAT-genotype. Nat. Biotechnol. 37, 907–915. [PubMed: 31375807]

Kimmel CB, Ballard WW, Kimmel SR, Ullmann B, and Schilling TF (1995). Stages of embryonic development of the zebrafish. Dev. Dyn. 203, 253–310. [PubMed: 8589427]

Kochupurakkal BS, Harari D, Di-Segni A, Maik-Rachline G, Lyass L, Gur G, Kerber G, Citri A, Lavi S, Eilam R, et al. (2005). Epigen, the last ligand of ErbB receptors, reveals intricate relationships between affinity and mitogenicity. J. Biol. Chem. 280, 8503–8512. [PubMed: 15611079]

Koh AY, Köhler JR, Coggshall KT, Van Rooijen N, and Pier GB (2008). Mucosal damage and neutropenia are required for Candida albicans dissemination. PLoS Pathog. 4, e35. [PubMed: 18282097]

Kwong RW, and Perry SF (2013). The tight junction protein claudin-b regulates epithelial permeability and sodium handling in larval zebrafish, Danio rerio. Am. J. Physiol. Regul. Integr. Comp. Physiol. 304, R504–R513. [PubMed: 23364531]

Le Guellec D, Morvan-Dubois G, and Sire JY (2004). Skin development in bony fish with particular emphasis on collagen deposition in the dermis of the zebrafish (Danio rerio). Int. J. Dev. Biol. 48, 217–231. [PubMed: 15272388]

Lee SC, Li A, Calo S, Inoue M, Tonthat NK, Bain JM, Louw J, Shinohara ML, Erwig LP, Schumacher MA, et al. (2015). Calcineurin orchestrates dimorphic transitions, antifungal drug responses and host-pathogen interactions of the pathogenic mucoralean fungus Mucor circinelloides. Mol. Microbiol. 97, 844–865. [PubMed: 26010100]

Li H, Handsaker B, Wysoker A, Fennell T, Ruan J, Homer N, Marth G, Abecasis G, and Durbin R; 1000 Genome Project Data Processing Subgroup (2009). The Sequence Alignment/Map format and SAMtools. Bioinformatics 25, 2078–2079. [PubMed: 19505943]

Liao Y, Smyth GK, and Shi W (2014). featureCounts: an efficient general purpose program for assigning sequence reads to genomic features. Bioinformatics 30, 923–930. [PubMed: 24227677]

Liu M, Spellberg B, Phan QT, Fu Y, Fu Y, Lee AS, Edwards JE Jr., Filler SG, and Ibrahim AS (2010). The endothelial cell receptor GRP78 is required for mucormycosis pathogenesis in diabetic mice. J. Clin. Invest. 120, 1914–1924. [PubMed: 20484814]

Lo HJ, Köhler JR, DiDomenico B, Loebenberg D, Cacciapuoti A, and Fink GR (1997). Nonfilamentous C. albicans mutants are avirulent. Cell 90, 939–949. [PubMed: 9298905]

Lo HJ, Tseng KY, Kao YY, Tsao MY, Lo HL, and Yang YL (2015). Cph1p negatively regulates MDR1 involved in drug resistance in Candida albicans. Int. J. Antimicrob. Agents 45, 617–621. [PubMed: 25802233]

López-Muñoz A, Nicolás FE, García-Moreno D, Pérez-Oliva AB, Navarro-Mendoza MI, Hernández-Oñate MA, Herrera-Estrella A, Torres-Martínez S, Ruiz-Vázquez RM, Garre V, and Mulero V (2018). An Adult Zebrafish Model Reveals that Mucormycosis Induces Apoptosis of Infected Macrophages. Sci. Rep. 8, 12802. [PubMed: 30143654]

Love MI, Huber W, and Anders S (2014). Moderated estimation of fold change and dispersion for RNA-seq data with DESeq2. Genome Biol. 15, 550. [PubMed: 25516281]

Lubkov V, and Bar-Sagi D (2014). E-cadherin-mediated cell coupling is required for apoptotic cell extrusion. Curr. Biol. 24, 868–874. [PubMed: 24704076]

Author Manuscript Author Manuscript Author Manuscript Author Manuscript

Miguel JC, Maxwell AA, Hsieh JJ, Harnisch LC, Al Alam D, Polk DB, Lien CL, Watson AJ, and Frey MR (2017). Epidermal growth factor suppresses intestinal epithelial cell shedding through a MAPK-dependent pathway. J. Cell Sci. 130, 90–96. [PubMed: 27026527]

Moreno E, Valon L, Levillayer F, and Levayer R (2019). Competition for Space Induces Cell Elimination through Compaction-Driven ERK Downregulation. Curr. Biol. 29, 23–34.e8. [PubMed: 30554899]

Naidu MU, Ramana GV, Rani PU, Mohan IK, Suman A, and Roy P (2004). Chemotherapy-induced and/or radiation therapy-induced oral mucositis–complicating the treatment of cancer. Neoplasia 6, 423–431. [PubMed: 15548350]

Pankov R, and Yamada KM (2002). Fibronectin at a glance. J. Cell Sci. 115, 3861–3863. [PubMed: 12244123]

Pellettieri J, and Sánchez Alvarado A (2007). Cell turnover and adult tissue homeostasis: from humans to planarians. Annu. Rev. Genet. 41, 83–105. [PubMed: 18076325]

Pfaller MA, and Diekema DJ (2007). Epidemiology of invasive candidiasis: a persistent public health problem. Clin. Microbiol. Rev. 20, 133–163. [PubMed: 17223626]

Pignon JC, Grisanzio C, Geng Y, Song J, Shivdasani RA, and Signoretti S (2013). p63-expressing cells are the stem cells of developing prostate, bladder, and colorectal epithelia. Proc. Natl. Acad. Sci. USA 110, 8105–8110. [PubMed: 23620512]

Polk DB (1998). Epidermal growth factor receptor-stimulated intestinal epithelial cell migration requires phospholipase C activity. Gastroenterology 114, 493–502. [PubMed: 9496939]

Poplimont H, Georgantzoglou A, Boulch M, Walker HA, Coombs C, Papaleonidopoulou F, and Sarris M (2020). Neutrophil Swarming in Damaged Tissue Is Orchestrated by Connexins and Cooperative Calcium Alarm Signals. Curr. Biol. 30, 2761–2776.e7. [PubMed: 32502410]

Renshaw SA, Loynes CA, Trushell DM, Elworthy S, Ingham PW, and Whyte MK (2006). A transgenic zebrafish model of neutrophilic inflammation. Blood 108, 3976–3978. [PubMed: 16926288]

Rock JR, Randell SH, and Hogan BL (2010). Airway basal stem cells: a perspective on their roles in epithelial homeostasis and remodeling. Dis. Model. Mech. 3, 545–556. [PubMed: 20699479]

Rodrigues CF, Rodrigues ME, and Henriques M (2019). Candida sp. Infections in Patients with Diabetes Mellitus. J. Clin. Med. 8, 76.

Rosenblatt J, Raff MC, and Cramer LP (2001). An epithelial cell destined for apoptosis signals its neighbors to extrude it by an actin- and myosin-dependent mechanism. Curr. Biol. 11, 1847–1857. [PubMed: 11728307]

Schoen TJ, Rosowski EE, Knox BP, Bennin D, Keller NP, and Huttenlocher A (2019). Neutrophil phagocyte oxidase activity controls invasive fungal growth and inflammation in zebrafish. J. Cell Sci. 133, jcs236539.

Singh B, Fleury C, Jalalvand F, and Riesbeck K (2012). Human pathogens utilize host extracellular matrix proteins laminin and collagen for adhesion and invasion of the host. FEMS Microbiol. Rev. 36, 1122–1180. [PubMed: 22537156]

Sipsas NV, and Kontoyiannis DP (2012). Invasive fungal infections in patients with cancer in the Intensive Care Unit. Int. J. Antimicrob. Agents 39, 464–471. [PubMed: 22337064]

Strachan L, Murison JG, Prestidge RL, Sleeman MA, Watson JD, and Kumble KD (2001). Cloning and biological activity of epigen, a novel member of the epidermal growth factor superfamily. J. Biol. Chem. 276, 18265–18271. [PubMed: 11278323]

Tatara AM, Wurster S, Lockworth CR, Albert ND, Walsh TJ, Mikos AG, Eisenhoffer GT, and Kontoyiannis DP (2018). Immunosuppressed Adult Zebrafish Model of Mucormycosis. Antimicrob. Agents Chemother. 62, e00698–18. [PubMed: 30150461]

Teo JL, Tomatis VM, Coburn L, Lagendijk AK, Schouwenaar IM, Budnar S, Hall TE, Verma S, McLachlan RW, Hogan BM, et al. (2020). Src kinases relax adherens junctions between the neighbors of apoptotic cells to permit apical extrusion. Mol. Biol. Cell 31, 2557–2569. [PubMed: 32903148]

Thakur PC, Davison JM, Stuckenholz C, Lu L, and Bahary N (2014). Dysregulated phosphatidylinositol signaling promotes endoplasmic-reticulum-stress-mediated intestinal mucosal injury and inflammation in zebrafish. Dis. Model. Mech. 7, 93–106. [PubMed: 24135483]

Author Manuscript Author Manuscript Author Manuscript Author Manuscript

Turksen K, and Troy TC (2004). Barriers built on claudins. J. Cell Sci. 117, 2435–2447. [PubMed: 15159449]

Vehreschild JJ, Birtel A, Vehreschild MJ, Liss B, Farowski F, Kochanek M, Sieniawski M, Steinbach A, Wahlers K, Fätkenheuer G, and Cornely OA (2013). Mucormycosis treated with posaconazole: review of 96 case reports. Crit. Rev. Microbiol. 39, 310–324. [PubMed: 22917084]

Vicentini AP, Gesztesi JL, Franco MF, de Souza W, de Moraes JZ, Travassos LR, and Lopes JD (1994). Binding of Paracoccidioides brasiliensis to laminin through surface glycoprotein gp43 leads to enhancement of fungal pathogenesis. Infect. Immun. 62, 1465–1469. [PubMed: 8132354]

Voelz K, Gratacap RL, and Wheeler RT (2015). A zebrafish larval model reveals early tissue-specific innate immune responses to Mucor circinelloides. Dis. Model. Mech. 8, 1375–1388. [PubMed: 26398938]

Walsh TJ, Hospenthal DR, Petraitis V, and Kontoyiannis DP (2019). Necrotizing Mucormycosis of Wounds Following Combat Injuries, Natural Disasters, Burns, and Other Trauma. J. Fungi (Basel) 5, 57.

Wang J (2018). Neutrophils in tissue injury and repair. Cell Tissue Res. 371, 531–539. [PubMed: 29383445]

Watkins TN, Gebremariam T, Swidergall M, Shetty AC, Graf KT, Alqarihi A, Alkhazraji S, Alsaadi AI, Edwards VL, Filler SG, et al. (2018). Inhibition of EGFR Signaling Protects from Mucormycosis. MBio 9, e01384–18. [PubMed: 30108171]

Webb AE, and Kimelman D (2005). Analysis of early epidermal development in zebrafish. Methods Mol. Biol. 289, 137–146. [PubMed: 15502179]

Wurster S, Kumaresan PR, Albert ND, Hauser PJ, Lewis RE, and Kontoyiannis DP (2019). Live Monitoring and Analysis of Fungal Growth, Viability, and Mycelial Morphology Using the IncuCyte NeuroTrack Processing Module. MBio 10, e00673–19. [PubMed: 31138745]

Xu S, Webb SE, Lau TCK, and Cheng SH (2018). Matrix metalloproteinases (MMPs) mediate leukocyte recruitment during the inflammatory phase of zebrafish heart regeneration. Sci. Rep. 8, 7199. [PubMed: 29740050]

Yoshinari N, Ishida T, Kudo A, and Kawakami A (2009). Gene expression and functional analysis of zebrafish larval fin fold regeneration. Dev. Biol. 325, 71–81. [PubMed: 18950614]

Author Manuscript Author Manuscript Author Manuscript Author Manuscript

Highlights

- Inducible epithelial cell loss allows modeling of fungal infection in zebrafish larvae
- Extrusion of numerous cells exposes laminin and increases fungal adhesion and invasion
- Cell extrusion stimulates *epigen*, *mmp13a*, and *il1b* expression and neutrophil recruitment
- rhEPGN suppresses extrusion to provide protective effects against fungal invasion

Author Manuscript Author Manuscript Author Manuscript Author Manuscript

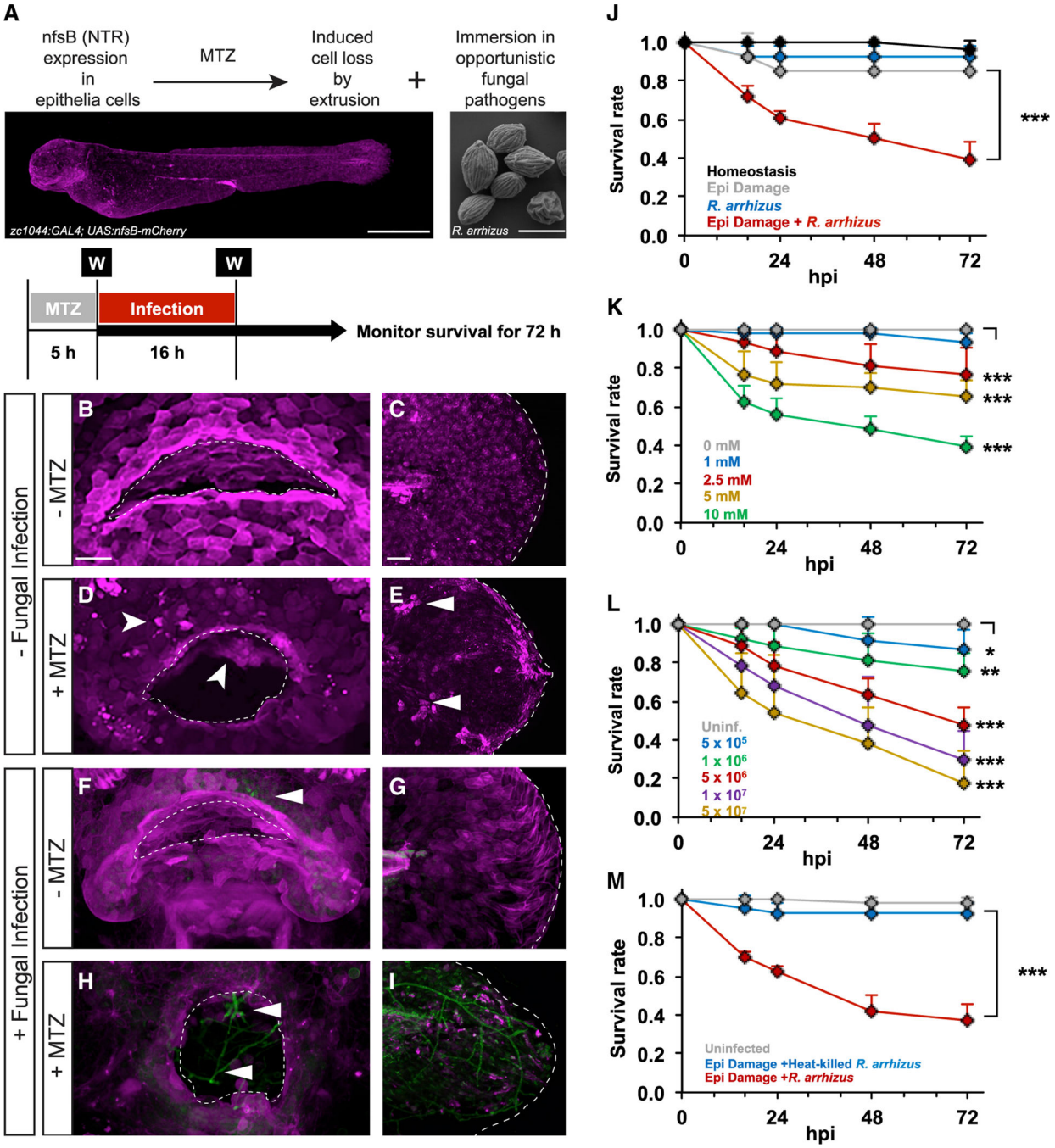

Figure 1. A model of invasive fungal infection mediated by inducible epithelial cell loss

(A) Schematic of a 4 days post fertilization (dpf) zebrafish larva (scale bar, 500 μm); scanning electron microscopy (SEM) image of *Rhizopus arrhizus* (clinical isolate 749) spores prior to immersion with larvae (scale bar, 5 μm); and timeline of addition and removal of MTZ to induce epithelial damage, addition of 5×10^6/mL *R. arrhizus* spores for 16 h, and survival monitoring. W, triple wash step.

(B–I) Maximum intensity projections of confocal images for (B–I) NTR-mCherry and (F–I) *Rhizopus arrhizus*-GFP in the orofacial region and tail fin of 5 dpf larvae under homeostatic

Author Manuscript Author Manuscript Author Manuscript Author Manuscript

conditions (B, C, F, and G) and after epithelial damage (D, E, H, and I). Arrowheads in (D) and (E) denote cell extrusion events, and arrowheads in (F) and (H) denote fungal spore attachment and hyphal growth, respectively. Scale bars, 40 μm.

(J) Larva survival curves after *Rhizopus* infection under homeostatic conditions and with tissue damage (n = 27–28 per condition).

(k) Survival rates of *R. arrhizus*-infected larvae with differential intensity of tissue damage (n = 43 per MTZ concentration).

(L) Larva survival curves after tissue damage and exposure to differential amounts of *R. arrhizus* spores (n = 31–33 per inoculum).

(M) Survival rates of larvae with mucosal damage infected with 5×10^6 heat-inactivated (30 min, 100 C) or vital *R. arrhizus* 749 spores (n = 42 per condition).

(J–M) Aggregated survival rates across three independent experiments are plotted. Error bars represent SD; Mantel-Cox log rank test.

Author Manuscript Author Manuscript Author Manuscript Author Manuscript

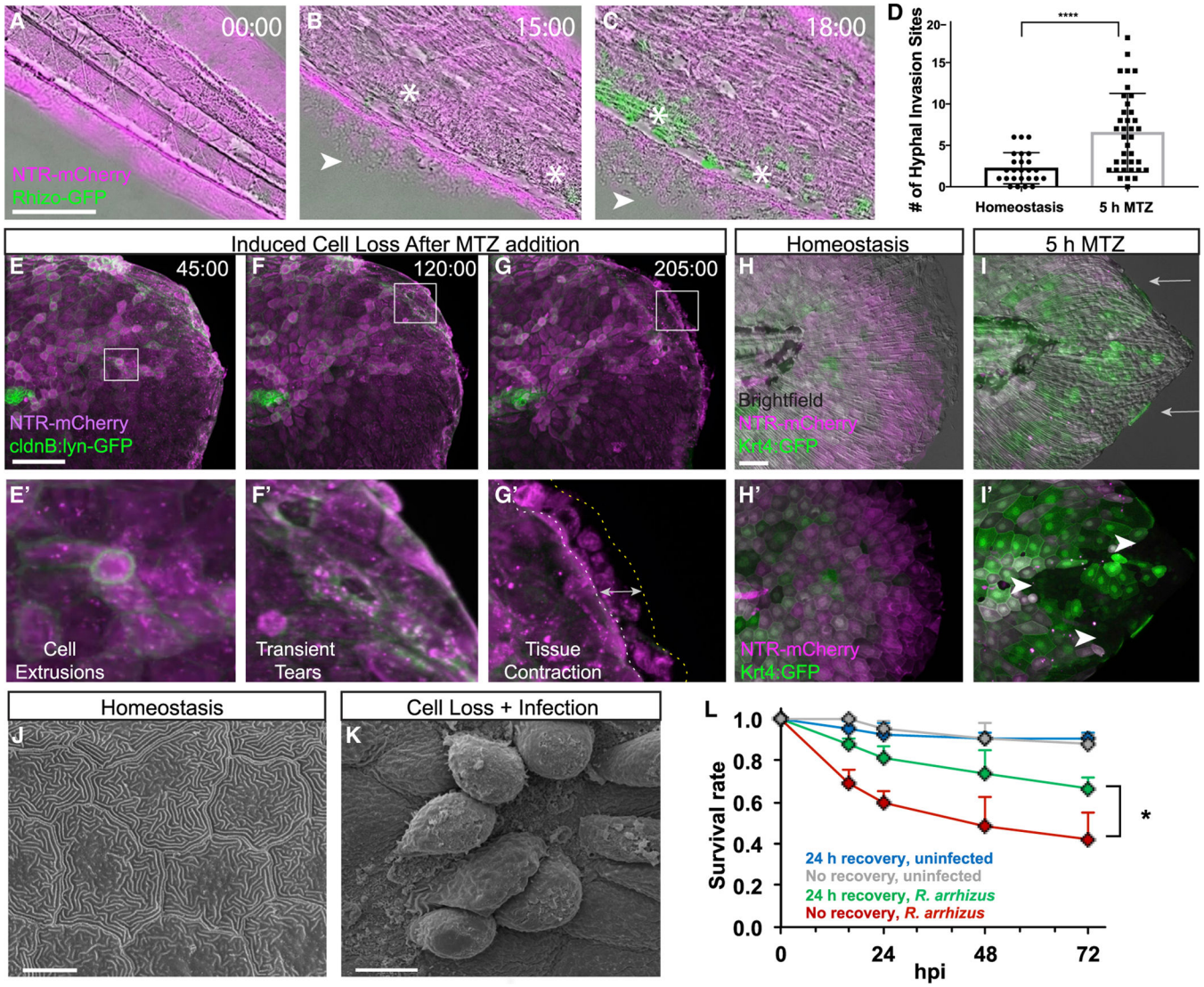

Figure 2. Continual epithelial cell extrusion compromises barrier integrity and leads to lethal fungal invasion

(A–C) Fluorescence images for NTR-mCherry and *Rhizopus arrhizus*-GFP in the tail fin of 5 dpf larvae after epithelial damage. Arrowheads denote epithelial tissue damage, and asterisks mark the fungus. Scale bar, 200 μm.

(D) Mean number of hyphal invasion sites per larva. Hyphal invasion sites were quantified in 37 MTZ-treated larvae and 25 larvae during epithelial homeostasis from 2 independent experiments. Error bars represent SEM; unpaired two-sided t test.

(E–G) Maximum intensity projections of confocal images of induced epithelial extrusion and subsequent tissue damage over time (NTR-mCherry and cldnB:lyn-GFP). Boxes denote regions shown below. Double arrowheads denote amounts of tissue contraction. Scale bars, 100 μm.

(H and I) Maximum intensity projections of confocal images of homeostatic epithelium and epithelial tissue damage after MTZ treatment (NTR-mCherry and Krt4:GFP). Arrows denote

areas of tissue contraction. Arrowheads denote regions with epithelial gaps. Scale bar, 20 μm.

(J and K) SEM image of *R. arrhizus 749* spores during invasion after mucosal damage. Scale bars, 10 μm.

(L) Survival rates of larvae infected with *R. arrhizus 749* spores immediately after epithelial damage or after a 24-h recovery period, a time point when the epithelial tissue tears and gaps have largely resolved. Aggregated survival rates based on 42–45 larvae per condition across three independent experiments are plotted. Error bars represent SD; Mantel-Cox log rank test.

Author Manuscript Author Manuscript Author Manuscript Author Manuscript

Author Manuscript Author Manuscript Author Manuscript Author Manuscript

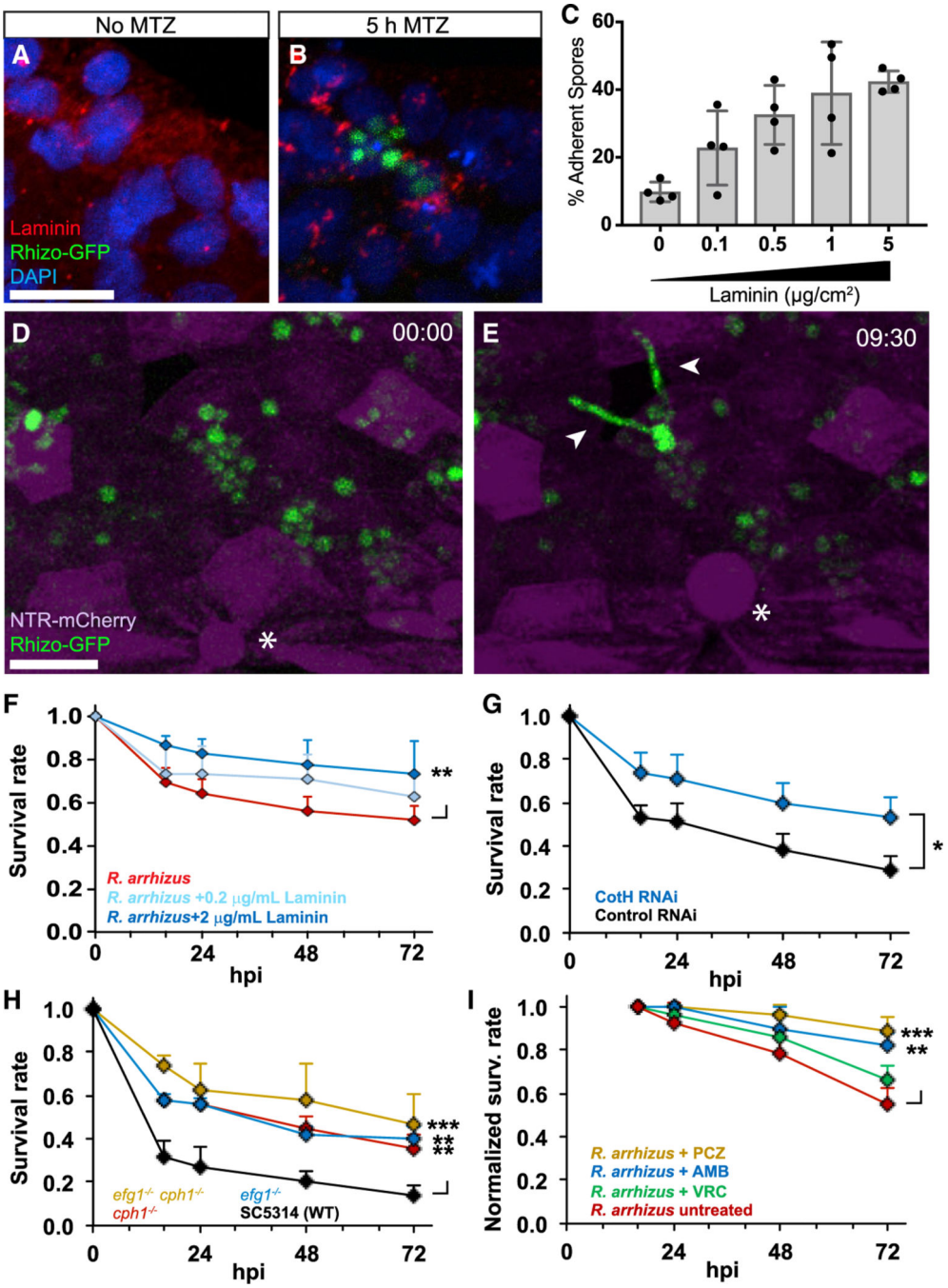

Figure 3. Fungal spores adhere to damaged epithelia and initiate hyphal growth

(A and B) Maximum intensity projections of confocal images of *R. arrhizus*-GFP spores adhered to areas of damaged epithelial tissue with exposed laminin compared with homeostatic epithelium. Scale bar, 20 µm.

(C) Quantification of spore adherence to wells coated with increasing concentrations of laminin.

Author Manuscript Author Manuscript Author Manuscript Author Manuscript

(D and E) Time-lapse imaging of *R. arrhizus*-GFP spores adhered at sites of epithelial damage undergoing germination. Arrowheads denote germlings/early hyphae. Asterisks denote epithelial cell extrusion. Scale bar, 20 μm.

(F) Survival rates of larvae with induced cell loss infected with *R. arrhizus* 749 spores pre-coated or not with 0.2 or 2 μg/mL laminin. Aggregated survival rates based on 75 larvae per condition across five independent experiments, and SDs are plotted.

(G) Survival rates of larvae with induced cell loss after addition of CotH-depleted *R. arrhizus* (CotHRNAi) and the corresponding wild-type control (control RNAi).

(H) Survival rates of larvae with induced cell loss after addition *efg1*, *cph1*, or *efg1/cph1 C. albicans* mutants compared with an isogenic control (SC5314). Aggregated survival rates based on 44–45 larvae per condition across three independent experiments are plotted. Error bars represent SD.

(I) Survival rates of larvae after induced cell loss after *R. arrhizus* infection and treatment with voriconazole (VRC), amphotericin B (AMB), and posaconazole (PCZ), normalized to the number of animals alive at the time of treatment (16 h post infection, n = 50–52 across five independent experiments).

(F–I) Mantel-Cox log rank test.

Author Manuscript Author Manuscript Author Manuscript Author Manuscript

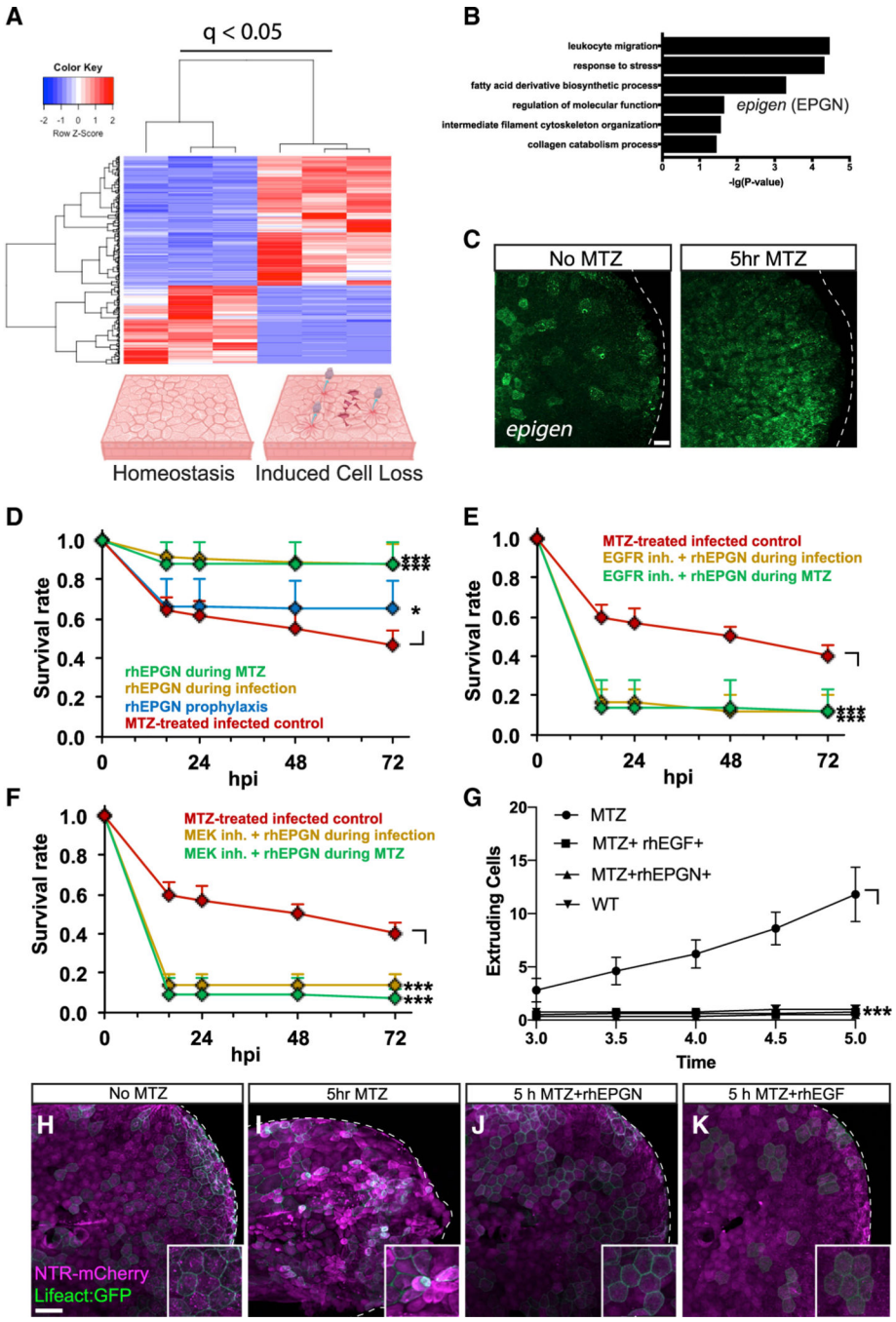

Figure 4. Treatment with rhEPGN suppresses epithelial cell extrusion and attenuates invasive fungal infection

(A) Heatmap of differentially expressed genesbetween homeostatic conditions (no MTZ) and induced epithelial cell loss by extrusion (MTZ-treated). q < 0.05, adjusted p value, Deseq2 and Benjamini-Hochberg method for FDR correction, three independent biological replicates, 15–30 larvae per replicate.

(B) Gene Ontology (GO) analysis of gene categories enriched after epithelial cell loss.

(C) Maximum intensity projections of fluorescent in situ hybridization for epigen in larvae with induced cell loss compared with homeostasis. Scale bar, 20 μm.

Author Manuscript Author Manuscript Author Manuscript Author Manuscript

(D–F) Larval survival after treatment with rhEPGN (D), rhEPGN and the EGFR inhibitor AG1478 (E), or rhEPGN and the MEK inhibitor U0126 (F) at different times during induction of damage and infection. Aggregated survival rates based on five (D, n = 72–74 per condition) or three independent experiments (E and F, n = 42–43 per condition), respectively, are plotted. Error bars represent SD; Mantel-Cox log rank test.

(G) Quantification of the number of extruding cells with and without rhEPGN or rhEGF treatment during induced damage. Data are from three independent experiments, and error bars represent SD; ***$p < 0.001$; ordinary one-way analysis of variance (ANOVA) with Dunnett's multiple comparisons test.

(H–K) Maximum intensity projections of confocal still images of a time-lapse sequence after induction of epithelial cell loss (H and I) and during treatment with rhEPGN (J) or rhEGF (K). Scale bar, 50 μm.

Author Manuscript Author Manuscript Author Manuscript Author Manuscript

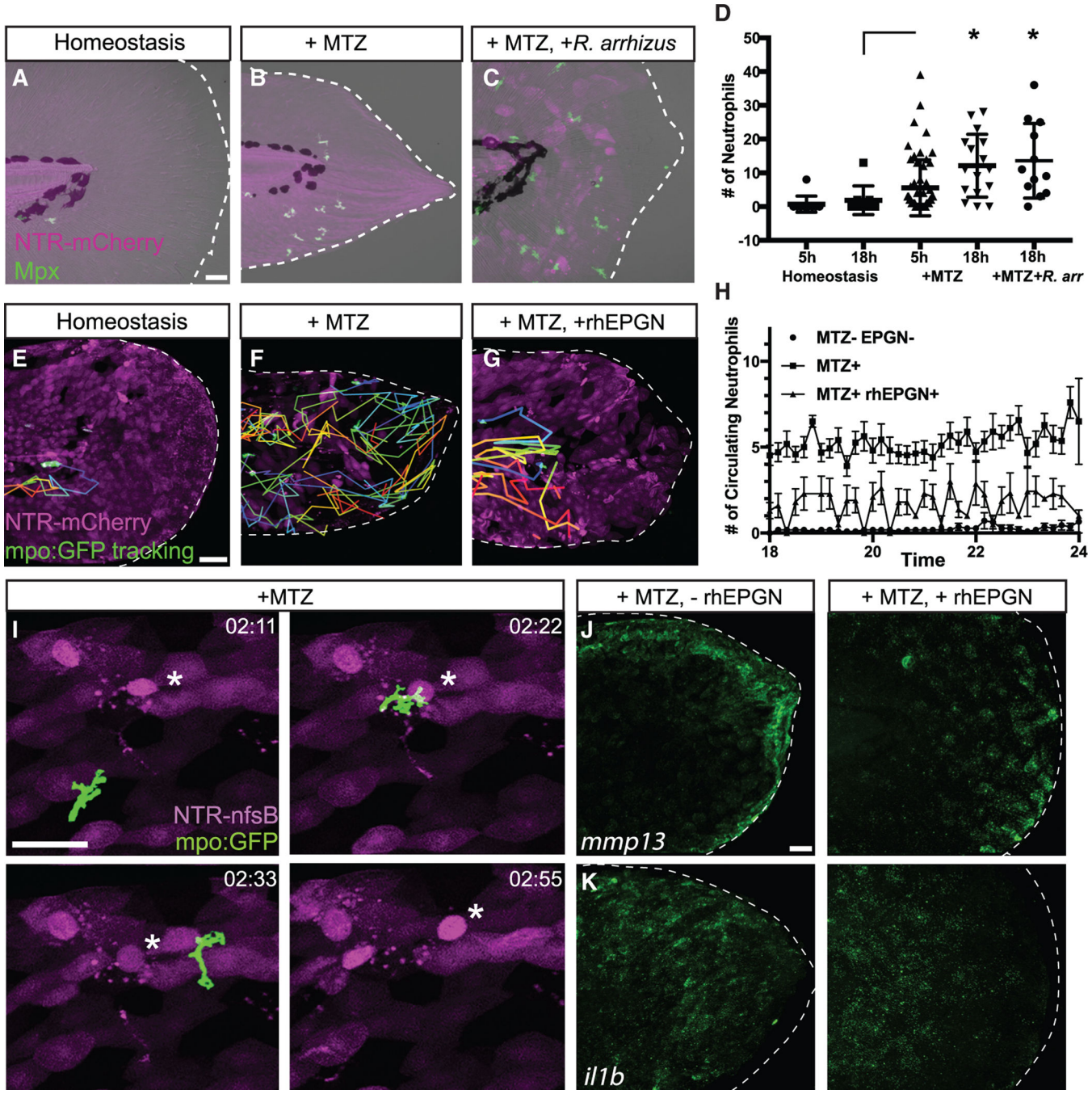

Figure 5. Neutrophils are recruited to sites of mucosal damage and invasive fungal infection

(A–C) Maximum intensity projections of confocal images of larvae stained for the neutrophil marker mpx (green) during homeostasis (A), after mucosal damage (B), and mucosal damage and *Rhizopus* infection. Scale bar, 20 μm.

(D) Quantification of the total number of neutrophils present in the epithelium (n = 108 number of animals).

(E–G) Still images from time-lapse videos of neutrophil dynamics after cell loss-induced mucosal damage and after treatment with hrEPGN to suppress extrusion. Scale bar, 50 μm.

Author Manuscript Author Manuscript Author Manuscript Author Manuscript

(H) Quantification of the number of circulating neutrophils with and without rhEPGN or rhEGF treatment during induced damage. Data are from 38 animals from three independent experiments. Error bars represent SD.

(I) Still images from time-lapse videos of a neutrophil migrating to a site of extrusion (denoted by asterisks).

(J and K) Maximum intensity projection images of fluorescent *in situ* hybridization for *mmp13a* and *il1b* in larvae with induced cell loss compared with those treated with hrEPGN. Scale bar, 20 μm.

Author Manuscript Author Manuscript Author Manuscript Author Manuscript

KEY RESOURCES TABLE

REAGENT or RESOURCE	SOURCE	IDENTIFIER
Antibodies		
Rabbit Anti-Active Caspase-3	BD Biosciences	Cat# 559565; RRID: AB_397274
Rat Anti-BrdU	AbCam	Cat# Ab6326; RRID: AB_305426
Rabbit Anti-Tp63	Genetex	Cat# GTX124660; RRID: AB_11175363
Rabbit Anti-Laminin	Sigma-Aldrich	Cat# L9393; RRID: AB_477163
Rabbit Anti-Mpx	GeneTex	Cat# GTX128379, RRID: AB_2885768
Chemicals, peptides, and recombinant proteins		
Posaconazole	Toronto Research Chemicals	P689600
Voriconazole	Sigma-Aldrich	32483
Amphotericin B	Sigma-Aldrich	46006
Human laminin purified protein	Sigma-Aldrich	AG56P
Recombinant human laminin 521	Thermo Fisher	A29249
Fibronectin	Sigma-Aldrich	F0895
Sphingosine kinase 1 inhibitor (Ski5C)	Sigma-Aldrich	S8326
Sphingosine kinase 1 inhibitor (Ski5C) CAY1062	Cayman Chemical	13371
Sphingosine kinase 1 inhibitor (Ski5C)	Santa Cruz	SC-288340
Recombinant Human EGF	Prospec Bio	CYT-217-b
Recombinant Human Epigen	Peptides International	CYT-601
EGF Receptor Inhibitor AG1478	EMD Millipore	658552
MEK Inhibitor U0126	EMD Millipore	662005
Metronidazole	Sigma-Aldrich	M-3761
DAPI	Thermo Fisher	D1306
Tricaine-S	Western Chemical	TRICMGR0100
Tween-20	Sigma-Aldrich	P9416
SSC Buffer 20X Concentrate	Sigma-Aldrich	S6639
Critical commercial assays		
DNeasy Blood and Tissue Kit	QIAGEN	69506
TaqMan Universal PCR Master Mix	Applied Biosystems / Thermo Fisher Scientific	4304437
RNeasy Kit	QIAGEN	74104
DNase Kit	QIAGEN	79254
HCR v3.0 Custom Probe Set epigen	Molecular Instruments	Accession: XM_001344355.8
HCR v3.0 Custom Probe Set il1b	Molecular Instruments	Accession: NM_212844.2
HCR v3.0 Custom Probe Set cxcl8B	Molecular Instruments	NM_001327985.1
HCR v3.0 Custom Probe Set mmp13a	Molecular Instruments	Accession: NM_001290479.1
HCR Amplifier B1	Molecular Instruments	HCR Amplifier
HCR whole-mount probe hybridization buffer	Molecular Instruments	HCR whole-mount probe hybridization buffer
HCR whole-mount probe wash buffer	Molecular Instruments	HCR whole-mount probe wash buffer

Author Manuscript Author Manuscript Author Manuscript Author Manuscript

REAGENT or RESOURCE	SOURCE	IDENTIFIER
HCR whole-mount amplification buffer	Molecular Instruments	HCR whole-mount amplification buffer
Biomasher II tubes	Nippi	320103
Low Melt Agarose	Invitrogen	16520
MatTek Glass Bottom Dish	MatTek	P35G-1.0–20-C
Deposited data		
RNaseq Raw Data	NIH Gene Expression Omnibus	GEO: GSE140839
Experimental models: organisms/strains		
Zebrafish: *Et(Gal4-VP16)^{zc1044A}, Tg(UAS-1b:nsfB-mCherry)^{c264}*	Eisenhoffer et al., 2017	*zc1044A*
Zebrafish: *Et(Gal4-VP16)^{zc1036A}, Tg(UAS-1b:nsfB-mCherry)^{c264}*	Eisenhoffer et al., 2017	*zc1036A*
Zebrafish: *Et(Gal4-VP16)^{zc1044A}, Tg(UAS1b:nsfB-mCherry)^{c264}, Tg(UAS-1b:Lifeact-EGFP)^{utm1}*	Eisenhoffer et al., 2017	*utm1*
Zebrafish: *Tg(Krt4:GFP)*	Gong et al., 2002	N/A
Zebrafish: *Tg(8.0cldnb:lynEGFP)^{zf106}*	Haas and Gilmour, 2006	*zf106*
Candida albicans Y4215	MD Anderson Cancer Center (clinical collection)	Ca-*Y4215*
Candida albicans homozygous cph1 mutant	J. L. Lopez-Ribot, the University of Texas at San Antonio (Lo et al., 1997)	*cph1$^{-/-}$*
Candida albicans homozygous efg1 mutant	J. L. Lopez-Ribot, the University of Texas at San Antonio (Lo et al., 1997)	*efg1$^{-/-}$*
Candida albicans homozygous cph1 and efg1 double mutant	J. L. Lopez-Ribot, the University of Texas at San Antonio (Lo et al., 1997)	*cph1$^{-/-}$ efg1$^{-/-}$*
Candida albicans SC5314	J. L. Lopez-Ribot, the University of Texas at San Antonio (Lo et al., 1997)	*SC5314*
Mucor circinelloides 518	MD Anderson Cancer Center (clinical collection)	*Mc-518*
Rhizopus arrhizus 749	MD Anderson Cancer Center (clinical collection)	*Ra-749*
Rhizopus arrhizus (FTR1)-GFP	A. S. Ibrahim, University of California, Los Angeles,	*Rhizo-GFP*
Rhizopus arrhizus Control (empty) RNAi	A. S. Ibrahim, University of California, Los Angeles (Gebremariam et al., 2014; (Ibrahim et al., 2010))	*Control RNAi*
Rhizopus arrhizus CotH RNAi	A. S. Ibrahim, University of California, Los Angeles (Gebremariam et al., 2014)	*CotH RNAi*
Oligonucleotides		
R. arrhizus 18S forward amplification primer, GCGGATCGCATGGCC	Applied Biosystems / Thermo Fisher Scientific (Ibrahim et al., 2005)	N/A
R. arrhizus 18S reverse amplification primer, CCATGATAGGGCAGAAAATCG	Applied Biosystems / Thermo Fisher Scientific (Ibrahim et al., 2005)	N/A

Author Manuscript Author Manuscript Author Manuscript Author Manuscript

REAGENT or RESOURCE	SOURCE	IDENTIFIER
R. arrhizus 18S hybridization probe, FAM-TGTGCCGGCGACGGTCCAC-TAMRA	Applied Biosystems / Thermo Fisher Scientific (Ibrahim et al., 2005)	N/A
Software and algorithms		
R (version 3.6.0)	R core Team	https://www.R-project.org/
R Studio (version 1.2.5033)	R Studio Team	https://www.rstudio.com/
FastQC (version 0.11.8)	N/A	https://www.bioinformatics.babraham.ac.uk/projects/fastqc/
Trimmomatic (version 0.33)	Bolger et al., 2014	http://www.usadellab.org/cms/?page=trimmomatic
HiSat2 (version 2.0.4)	Kim et al., 2019	http://daehwankimlab.github.io/hisat2/
Zebrafish genome (GRCz11)	NCBI	GenBank: GCA_000002035.4
Samtools (version 1.8)	Li et al., 2009	https://github.com/samtools/samtools
Featurecounts (1.6.3)	Liao et al., 2014	http://subread.sourceforge.net/
DeSeq2 (version 1.24)	Love et al., 2014	http://bioconductor.org/packages/release/bioc/html/DESeq2.html
GOEnrichment	N/A	https://github.com/DanFaria/GOEnrichment
GraphPad Prism (version 7.03)	Graphpad	https://www.graphpad.com/scientific-software/prism/
Zeiss Zen Blue 2.6	Zeiss	https://www.zeiss.com/microscopy/us/products/microscope-software/zen.html
Olympus FV312S-SW	Olympus	https://www.olympus-lifescience.com/en/support/downloads/
IncuCyte ZOOM software (version 2016B)	Sartorius / Essen Bioscience	https://www.essenbioscience.com/en/products/software/